Analysis on ignition kernel formation in a quiescent mixture: different characteristic time scales and critical heating powers

Dehai Yu, Xinyi Chen and Zheng Chen*

SKLTCS, CAPT, Department of Mechanics and Engineering Science, College of Engineering, Peking University, Beijing 100871, China

Abstract

Flame ignition is one of the most fundamental and ubiquitous problems in the field of combustion. Flame ignition in a quiescent flammable mixture consists of two phases: ignition kernel formation and subsequent transition to self-sustained expanding spherical flame. Most of previous studies focused on the second phase while little attention was paid to the first phase. In this work, theoretical analysis is conducted for ignition kernel formation induced by external heating within finite domain and finite duration. The ignition kernel formation consists of three stages, i.e., onset of thermal runaway, generation of reaction front at the center, and arrival of reaction front at the edge of heating domain. The characteristic time scales for these three stages are evaluated. Good agreement between theoretical analysis and transient simulation has been obtained. The delay times for the generation of reaction front at the center and its propagation to the edge of heating domain decrease rapidly with the external heating power density; and the delay time for thermal runaway is the primary component in the total time for ignition kernel formation. Moreover, a minimum power density for external heating below which thermal runaway cannot occur is determined. Since chemical reaction is self-sustained by releasing heat, two additional threshold values of external heating power densities are determined respectively corresponding to spontaneous generation of reaction front at the center and its subsequent propagation across the edge of heating domain. This study provides useful insights into ignition kernel formation occurring in premixed flame ignition.

Keywords: Ignition; thermal runaway; reaction front; characteristic time scale; heating power density

---

* Corresponding author, Email address: cz@pku.edu.cn, Tel: 86-10-62766232

1. Introduction

In combustion devices, forced ignition is widely adopted to guarantee the overall performance and reliability [1-3]. Recently, the rising concern on environmental protection has promoted increasing demand in developing high-efficiency, low-emission combustion techniques, such as burning exceedingly lean stratified fuel/air mixtures or mixtures diluted by exhausted gas recirculation [1, 4, 5]. Under ultra-lean and highly diluted conditions, the mixtures are less reactive and thereby more difficult to be ignited. To ensure reliable ignition under these extreme conditions, it is crucial to understand the fundamental mechanisms controlling the ignition process.

Forced ignition refers to the generation of self-sustained flame in a combustible mixture by external thermal energy deposition. For gaseous mixture subject to point heating source, Vázquez-Espí and Liñán [6, 7] identified the non-diffusive and thermal-diffusive ignition regimes by comparing the relevant time scales involved in the ignition process. The relevant time scales include: (a) the acoustic time, t_a, describing the relaxation to mechanical equilibrium, (b) the heat conduction time, t_c, describing relaxation to thermal equilibrium, and (c) homogeneous ignition delay time, t_{ch}, representing reactivity of mixture [6, 7]. The non-diffusive ignition regime refers to $t_{ch} \cong t_a \ll t_c$, in which heat release from chemical reaction is balanced by expansion. In the thermal-diffusive regime, it suggests that $t_a \ll t_{ch} \cong t_c$, i.e., the heat loss during ignition is primarily due to heat conduction. Usually, the heating duration of spark discharge is considerably longer than the acoustic time scale [4, 8]. This means that forced ignition usually lies in the thermal-diffusive regime. In such situations, the pressure wave resulting from heat addition can hardly change the local chemical reaction rate [7] . Accordingly, the forced ignition occurs under near isobaric condition despite that a pressure wave could be produced at the instant of ignition energy deposition [7]. For transient external heating in finite spatial dimension, Kassoy [9] conducted a theoretical study considering the evolution of inert gas in the near field, which was found to be fundamentally affected by the ratio of energy deposition relative to the initial internal energy in the heated gas. However, chemical reaction was not considered by Kassoy [9]. Efforts still need be devoted to understanding the transient ignition process.

In general, the flame initiation process in a quiescent flammable mixture consists of two phases: (1) the establishment of an ignition kernel and (2) the transition of this ignition kernel to self-sustained expanding spherical flame which is popularly used to measure the laminar burning velocities for different fuels under different thermal conditions [10-12]. The second phase requires the expanding flame kernel to traverse the critical ignition radius, which relies on the diffusional supply of reactant to the flame front, and thus is affected by the Lewis number of the combustible mixture [13]. Existing studies [13-15] have demonstrated that the critical ignition radius and minim ignition energy increase rapidly with Lewis number, which manifests the challenge of ignition in combustible mixture with large Le. Accordingly, recent attempts were made to facilitate the process of premixed flame initiation by lowering the Lewis number of the reactant mixture [16, 17]. For combustible mixture with sufficiently small Lewis number, flame kernel with short radius could still be found beyond the flammability [18], since the differential diffusion enhances the reaction capability at the flame front due to positive stretch. In such situation, the flame may quench at some distance because the flame intensity reduces as the flame kernel expands outwards [18].

For premixed reactant with Lewis number below unity, i.e., $Le \leq 1$, the critical ignition radius is identical to the flame ball radius [19, 20]. It was proved that the adiabatic flame ball is absolutely unstable [14] and that a positive displacement in flame radius leads to unbounded propagation of the flame front and thereby generates a self-sustained expanding spherical flame. However, in mixtures with $Le > 1$, the critical ignition radius tends to be smaller than the flame ball radius and larger than the flame thickness [13, 21]. Consequently, the minimum ignition energy (MIE) is greatly over-predicted (under-predicted) based on the flame ball radius (the flame thickness) for mixtures with large Lewis numbers.

Over the past a few decades, theoretical studies have been comprehensively conducted to understand the transition from initial ignition kernel to self-sustained expanding spherical flame [13-15, 18, 21-24]. The critical ignition radius can be identified as the radial distance at which the flame front has the smallest propagating velocity locally [13, 21, 25]. Chen et al. [13] demonstrated that the critical heating power is proportional to the cube of the critical ignition radius. Adopting large-activation-energy asymptotic analysis, Joulin [26] obtained an approximate nonlinear equation describing the temporal variation of flame front close to the stationary spherical flame subject to time-dependent heating source. Buckmaster and Joulin [27] examined the transient propagation of the self-extinguishing flame in combustible mixture with $Le < 1$ and clarified that the temporal evolution of flame radius follows $R \propto \sqrt{t}$, where t refers to time. Clavin [18] analyzed the dynamic quenching of spherical flame beyond flammability limits of planar flames, consistent with observation in micro-gravity experiments [19, 28]. In forced ignition by spark discharge, the flame front of the ignition kernel continues to propagate for a finite distance after the heating pulse is withdrawn, which is known as memory effect [6, 21, 26]. In our recent work [22, 29], a fully transient formulation was proposed and the transient effects on critical ignition radius and critical heating power were assessed. It was found that the memory effect of flame front propagation reduces the MIE [22].

The above studies have provided in-depth understanding on the transition of ignition kernel to self-sustained spherical flame. However, these studies did not give a complete description to the flame ignition process since the first phase, i.e., the ignition kernel formation, was not considered and instead a reaction front was introduced as initial conditions. Phenomenologically, the ignition kernel formation consists of three stages: (1) pure heating of combustible mixture before thermal runaway, (2) appearance of reactant front at the most reactive position (which is usually the center of the heating domain with the highest temperature), and (3) propagation of the reaction front towards the edge of heating domain, associated with continuous consumption of reactant. Being a highly transient process, the ignition kernel setup decisively affects the subsequent flame front propagation. In addition, the spark discharge is conventionally modeled by concentrated thermal energy deposition at the central point with zero dimension, which produces infinitely high temperature [15, 22, 30]. Such singularity infers that ignition kernel can be induced by arbitrarily low heating power, which unreasonably overestimates the ignitability of a combustible mixture by external heating.

To obtain a complete theory describing the forced ignition process and to feature the unsteady effects on forced ignition, it is desirable to conduct a theoretical investigation on the transient ignition kernel formation caused by external heating within finite domain and finite duration. No such attempt has been made in literature, which motivates the present study. This work shall provide detailed analysis on three stages, i.e., onset of thermal runaway, generation of reaction front and arrival of the reaction front to the edge of heating domain, involved in the ignition kernel formation. The emphasis is spent on the different characteristic time scales and critical heating powers involved in the ignition kernel formation.

The paper is organized as follows. In section 2, the governing equations describing the transient process of ignition kernel formation are presented. In section 3, the individual stages composing the ignition kernel formation are examined analytically with emphasis on determining their characteristic time scales. Besides, the effect of external heating power density on the ignition results are discussed in depth. The concluding remarks are presented in section 4.

2. Model and formulation

In this study, the forced ignition by spark discharge is modeled as thermal energy deposition during a finite time lapse within a finite domain. For simplicity, we consider the emergence and evolution of ignition kernel in a quiescent mixture. Since the size of heating domain is comparable with flame thickness, the heat transfer from the heating domain to the ambient reactant is dominated by heat conduction. The radiation effect tends to be secondary except for situations close to the flammability limit [31]. In general, the ignition kernel is very small and so is the volume of burned hot gas. Consequently, the radiation effect is not the dominant factor for the quenching of the flame kernel. The density variation may play a role during ignition process. Employing asymptotic analysis, Kassoy conducted theoretical studies considering spontaneous propagation of reaction wave originated from a finite hot spot [32]. By comparing the time scales of acoustic wave t_a and heat release from reaction t_{ch}, Kassoy [32] demonstrated that the density variation is negligible for $t_{ch}/t_a \ll 1$ (i.e., no time for thermal expansion during instantaneous heating) and is considerable for $t_{ch}/t_a \sim O(1)$. It is well known that the spark ignition consists of four phases, i.e., the pre-breakdown, breakdown, arc and glow discharge [33]. A spherical shock wave forms during the breakdown phase. The overall duration of the thermal energy addition in spark ignition (on order of millisecond) is much longer than the acoustic time scale (on order of microsecond), i.e., $t_{ch}/t_a \gg 1$ [33]. As the shock wave moving far away from the igniter, the pressure difference between the ignition kernel generated by the spark discharge and the cool reactant mixture in the ambience tends to be insubstantial. The isobaric condition suggests that the density in the ignition kernel due to external heating would be proportional to the local temperature, which is identical to the density variation across propagating flame induced by thermal expansion. According to Champion et al. [34], thermal expansion only has quantitative influence on the MIE and the main features of ignition are still recovered by using the thermal-diffusive model. For mathematical tractability, we therefore adopt the classical thermal-diffusive model, in which the thermal expansion is not considered and the density ρ, heat capacity c_p, thermal conductivity λ, mass diffusion coefficient of deficient reactant D, and heat of reaction q are assumed to be constant.

In theoretical analysis, it is conventional to consider one-step irreversible reaction. According to the Arrhenius law, the reaction rate is characterized by the reaction frequency factor B and the activation temperature T_a, i.e.,

$$\omega = \rho B Y e^{-T_a/T} \tag{1}$$

where Y is the mass fraction of the deficient reactant and T is the temperature of the mixture.

The governing equations describing the development of ignition kernel consist of conservation equations for thermal energy and deficient reactant, i.e.,

$$\rho c_p \frac{\partial T}{\partial t} = \frac{1}{r^2}\frac{\partial}{\partial r}\left(r^2 \lambda \frac{\partial T}{\partial r}\right) + \Phi(r,t) + q\omega \tag{2}$$

$$\rho \frac{\partial Y}{\partial t} = \frac{1}{r^2}\frac{\partial}{\partial r}\left(r^2 \rho D \frac{\partial Y}{\partial r}\right) - \omega \tag{3}$$

where Φ represents the rate of thermal energy deposition by spark discharge. The initial and boundary conditions are provided as follows:

$$\begin{cases} t = 0: & T = T_\infty, & Y = 1 \\ r = 0: & \partial T/\partial r = 0, & \partial Y/\partial r = 0 \\ r \to \infty: & T = T_\infty, & Y = 1 \end{cases} \tag{4}$$

For mathematical convenience, we assume that the external heating is imposed within a spherical domain of radius R_0 and lasts for a finite duration of t_0 with constant and uniform power density, denoted by Q_m. The total ignition energy is $E_{ig} = 4\pi R_0^3 t_0 Q_m/3$. Therefore, the rate of thermal energy deposition is described in the following form

$$\Phi(r,t) = Q_m[H(r) - H(r - R_0)][H(t) - H(t - t_0)] \tag{5}$$

where $H(x)$ refers to Heaviside step function, i.e.,

$$H(x) = \begin{cases} 0, & x < 0 \\ 1, & x \geq 0 \end{cases} \tag{6}$$

We define non-dimensional temperature and coordinates as follows

$$\theta = \frac{T - T_\infty}{T_\infty}, \qquad \tilde{r} = \frac{r}{R_0}, \qquad \tilde{t} = \frac{t}{R_0^2/\alpha} \tag{7}$$

where T_∞ refers to the temperature of unburned mixture far from the heating domain, and $\alpha = \lambda/\rho c_p$ is the thermal diffusivity of the mixture. The characteristic time of heat conduction, R_0^2/α, is used in the above non-dimensional variables. In terms of those non-dimensional quantities, the governing equations can be written in non-dimensional forms, i.e.,

$$\frac{\partial \theta}{\partial \tilde{t}} = \frac{1}{\tilde{r}^2}\frac{\partial}{\partial \tilde{r}}\left(\tilde{r}^2 \frac{\partial \theta}{\partial \tilde{r}}\right) + \tilde{Q}_m[H(\tilde{r}) - H(\tilde{r} - 1)][H(\tilde{t}) - H(\tilde{t} - \tilde{t}_0)] + \tilde{q}\tilde{B}Y \exp\left(-\frac{\theta_a + 1}{\theta + 1}\right) \tag{8}$$

$$\frac{\partial Y}{\partial \tilde{t}} = \frac{1}{Le}\frac{1}{\tilde{r}^2}\frac{\partial}{\partial \tilde{r}}\left(\tilde{r}^2 \frac{\partial Y}{\partial \tilde{r}}\right) - \tilde{B}Y \exp\left(-\frac{\theta_a + 1}{\theta + 1}\right) \tag{9}$$

where the additional non-dimensional quantities are defined as

$$\tilde{Q}_m = \frac{Q_m R_0^2}{\lambda T_\infty}, \qquad \theta_a = \frac{T_a - T_\infty}{T_\infty}, \qquad \tilde{t}_0 = \frac{t_0 \alpha}{R_0^2}, \qquad \tilde{q} = \frac{q}{c_p T_\infty}, \qquad \tilde{B} = \frac{B R_0^2}{\alpha}, \qquad Le = \frac{\alpha}{D} \tag{10}$$

Initially the reactant has constant and uniform temperature in the whole field, i.e., $\theta = 0$. After introducing the external heating given by equation (5), the temperature in the heated domain starts to increase. Because of symmetry, a plateau exists in profiles of both temperature and reactant mass fraction at the heating domain around $\tilde{r} = 0$. At distance sufficiently remote from the center, i.e., $\tilde{r} \gg 1$, the mixture can hardly feel the presence of external heating and thereby we have $\theta = 0$ and $Y = 1$. Therefore, the initial and boundary conditions for equations (8) and (9) are

$$\begin{cases} \tilde{t} = 0: & \theta = 0, & Y = 1 \\ \tilde{r} = 0: & \partial\theta/\partial\tilde{r} = 0, & \partial Y/\partial\tilde{r} = 0 \\ \tilde{r} \to \infty: & \theta = 0, & Y = 1 \end{cases} \tag{11}$$

The motion of the reaction front reveals the temporal and spatial variation of the nondimensional temperature and reactant mass fraction which are solved from equations (8) and (9). The propagation speed of the flame front could be exhibited by fixing the observing reference coordinate at the flame front and reformulating the governing equations. The detailed mathematical procedures can be found in the theoretical study by Chen and Ju [15].

3. Analysis on ignition kernel formation

As mentioned before, the establishment of ignition kernel consists of three stages: (1) pure heating of combustible mixture before thermal runaway, (2) appearance of reaction front due to depletion of reactant at the heating center, and (3) propagation of the reaction front to the edge of heating domain. Each stage is associated with a time scale, which is schematically shown in figure 1.

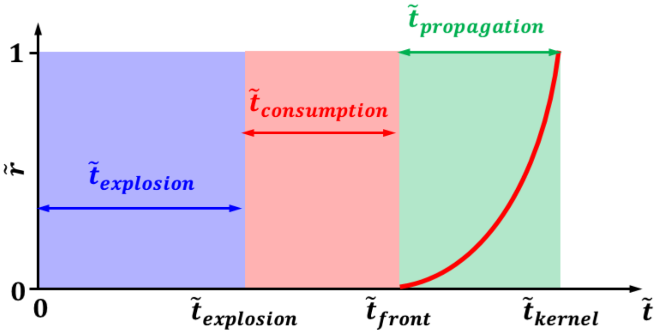

Figure 1 The schematic for the characteristic time scales involved in the ignition kernel formation. The red solid line indicates the propagation of reaction front from the center to the edge of ignition kernel.

Subject to external heating, the temperature at the heating center increases in the course of time. Therefore, thermal runaway is initiated at certain delay time, denoted by $\tilde{t}_{explosion}$, as shown in figure 1. Subsequent to thermal runaway, the consumption of reactant follows, and the time lapse for depletion of reactant at the center is denoted by $\tilde{t}_{consumption}$. The reaction front is characterized by the separation of reactant and product. Accordingly, the delay time for reaction front formation at the heating center, denoted by $\tilde{t}_{front}$, is the sum of those for thermal runaway and reactant depletion, i.e., $\tilde{t}_{front} = \tilde{t}_{explosion} + \tilde{t}_{consumption}$. The reaction front propagates outwardly. The time required for the arrival of reaction front at the edge of heating domain is denoted by $\tilde{t}_{propagation}$. Therefore, the total time lapse for the ignition kernel formation, denoted by $\tilde{t}_{kernel}$, is obtained as $\tilde{t}_{kernel} = \tilde{t}_{explosion} + \tilde{t}_{consumption} + \tilde{t}_{propagation}$. Note that all the time scales are normalized by the characteristic time of heat conduction, R_0^2/α, in which R_0 is the central heating radius and α is the thermal diffusivity of the mixture.

Due to heat release, chemical reaction is a self-sustained process. Subsequent to thermal runaway, the ignition kernel can develop spontaneously in the absence of constant external heating. In such situations, the ignition energy must be deposited by a single pulse with exceedingly short duration. Therefore, the heating power density must be sufficiently high. According to the degree of ignition kernel formation, three critical heating power densities can be defined, as shown in figure 2.

The first critical heating power density $Q_{cr,runaway}$ refers to the minimum rate of thermal energy deposition below which the thermal runaway can never occur in the combustible in spite of the constant presence of the external source. For $\tilde{Q}_m < \tilde{Q}_{cr,runaway}$ the thermal energy addition by external heating is completely balanced with conductive heat loss, and thereby chemical reaction can hardly be initiated. The second and third critical heating power densities $Q_{cr,front}$ and $Q_{cr,kernel}$ respectively characterize the appearance of reaction front and the subsequent propagation to the edge of heating domain. Those quantities are defined based on the condition that the external heating is withdrawn at the instant of thermal runaway. For $\tilde{Q}_{cr,runaway} < \tilde{Q}_m < \tilde{Q}_{cr,front}$, the chemical heat release is slower than conductive heat loss, thus the reaction soon terminates after thermal runaway. For $\tilde{Q}_{cr,front} < \tilde{Q}_m < \tilde{Q}_{cr,kernel}$, reaction front appears at the center. However, the propagation time of the reaction front tends to be so long that the temperature drop considerably lowers the local reactivity. Consequently, the reaction front may extinguish before arriving at $\tilde{r} = 1$. For $\tilde{Q}_m > \tilde{Q}_{cr,kernel}$, the strong pulse substantially increases the temperature in the heating domain and thereby induces successful ignition kernel formation.

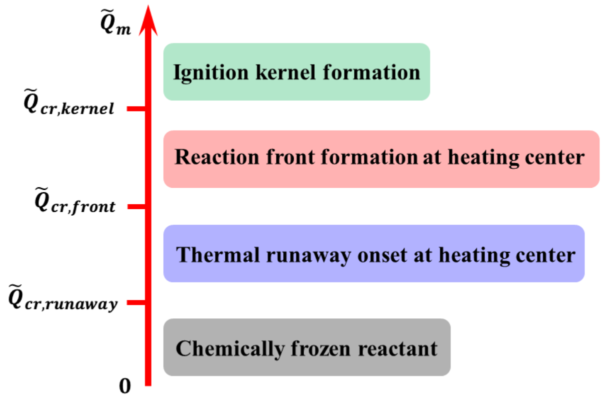

Figure 2 The schematic for different critical heating power densities. The central heating is removed at the onset of thermal runaway, i.e., $\tilde{t}_0 = \tilde{t}_{explosion}$.

In the following sections, we shall analyze the individual stages during ignition kernel formation with emphasis on evaluating the characteristic time scales and determining the critical heating power densities. It should be noted that final flame initiation refers to the transition of the established ignition kernel to self-sustained expanding spherical flame, which has been thoroughly underlined in existing studies [15, 21, 22]. The ignition kernel formation provides suitable initial condition for flame initiation and thereby is considered here.

3.1 Pre-ignition stage

Before ignition, heat release from chemical reaction tends to be negligible. Therefore, the chemical reaction term on the right-hand side of equations (8) and (9) can be neglected. Noticing that the heat release from the chemical reaction and thermal energy deposition by external source can vary independently in equation (8), we did not suppress the chemical reaction during the whole period of external heating. As seen in the following sections, the reaction heat release in association with external heating exhibit dominant impacts upon the occurrence of reaction front at the heating center and its subsequent propagation within the heating domain. The solution for Y subject to the above initial and boundary conditions is trivial, i.e., $Y = 1$ in the whole space. The energy equation can be simplified to

$$\frac{\partial \theta}{\partial \tilde{t}} = \frac{1}{\tilde{r}^2}\frac{\partial}{\partial \tilde{r}}\left(\tilde{r}^2 \frac{\partial \theta}{\partial \tilde{r}}\right) + \tilde{Q}_m[H(\tilde{r}) - H(\tilde{r}-1)][H(\tilde{t}) - H(\tilde{t}-\tilde{t}_0)] \tag{12}$$

which is a linear inhomogeneous partial differential equation of parabolic type. With the help of Green's function,

$$G(\tilde{r},\xi,\tilde{t})=\frac{\xi}{2\tilde{r}\sqrt{\pi\tilde{t}}}\left\{\exp\left[-\frac{(\tilde{r}-\xi)^2}{4\tilde{t}}\right]-\exp\left[-\frac{(\tilde{r}+\xi)^2}{4\tilde{t}}\right]\right\} \tag{13}$$

the general solution of equation (12) is obtained:

$$\theta(\tilde{r},\tilde{t})=\tilde{Q}_m\int_0^{\tilde{t}}\int_0^{\infty}[H(\tilde{r})-H(\tilde{r}-1)][H(\tilde{t})-H(\tilde{t}-\tilde{t}_0)]G(\tilde{r},\xi,\tilde{t}-\tau)d\xi d\tau \tag{14}$$

Substituting equation (13) into equation (14) yields the explicit expression for θ. Since the integrand has an abrupt change at $\tilde{t}=\tilde{t}_0$ and $\tilde{r}=1$, the spatial-temporal-integration is conducted in separate regimes and the transient variation of temperature profiles is in the following form:

For $\tilde{t}<\tilde{t}_0$ and $\tilde{r}<1$:

$$\begin{aligned}\theta=\frac{\tilde{Q}_m}{12\tilde{r}}\Bigg\{&6\tilde{r}-2\tilde{r}^3+2\sqrt{\tilde{t}/\pi}\,[(\tilde{r}-2)(\tilde{r}+1)+4\tilde{t}]\exp\left[-\frac{(\tilde{r}+1)^2}{4\tilde{t}}\right]\\&-2\sqrt{\tilde{t}/\pi}\,[(\tilde{r}-1)(\tilde{r}+2)+4\tilde{t}]\exp\left[-\frac{(\tilde{r}-1)^2}{4\tilde{t}}\right]\\&-[(\tilde{r}-1)^2(\tilde{r}+2)+6\tilde{r}\tilde{t}]\operatorname{erf}\left(\frac{\tilde{r}-1}{2\sqrt{\tilde{t}}}\right)+[(\tilde{r}-2)(\tilde{r}+1)^2+6\tilde{r}\tilde{t}]\operatorname{erf}\left(\frac{\tilde{r}+1}{2\sqrt{\tilde{t}}}\right)\Bigg\}\end{aligned} \tag{15}$$

For $\tilde{t}<\tilde{t}_0$ and $\tilde{r}>1$:

$$\begin{aligned}\theta=\frac{\tilde{Q}_m}{12\tilde{r}}\Bigg\{&4+2\sqrt{\tilde{t}/\pi}\,[(\tilde{r}-2)(\tilde{r}+1)+4\tilde{t}]\exp\left[-\frac{(\tilde{r}+1)^2}{4\tilde{t}}\right]\\&-2\sqrt{\tilde{t}/\pi}\,[(\tilde{r}-1)(\tilde{r}+2)+4\tilde{t}]\exp\left[-\frac{(\tilde{r}-1)^2}{4\tilde{t}}\right]\\&-[(\tilde{r}-1)^2(\tilde{r}+2)+6\tilde{r}\tilde{t}]\operatorname{erf}\left(\frac{\tilde{r}-1}{2\sqrt{\tilde{t}}}\right)+[(\tilde{r}-2)(\tilde{r}+1)^2+6\tilde{r}\tilde{t}]\operatorname{erf}\left(\frac{\tilde{r}+1}{2\sqrt{\tilde{t}}}\right)\Bigg\}\end{aligned} \tag{16}$$

For $\tilde{t}>\tilde{t}_0$:

$$
\begin{aligned}
\theta = \frac{\tilde{Q}_m}{12\tilde{r}}\Bigg\{ & 2\sqrt{\tilde{t}/\pi}\,[(\tilde{r}-2)(\tilde{r}+1)+4\tilde{t}]\exp\left[-\frac{(\tilde{r}+1)^2}{4\tilde{t}}\right] \\
& - 2\sqrt{\tilde{t}/\pi}\,[(\tilde{r}-1)(\tilde{r}+2)+4\tilde{t}]\exp\left[-\frac{(\tilde{r}-1)^2}{4\tilde{t}}\right] \\
& - [(\tilde{r}-1)^2(\tilde{r}+2)+6\tilde{r}\tilde{t}]\,\mathrm{erf}\left(\frac{\tilde{r}-1}{2\sqrt{\tilde{t}}}\right) + [(\tilde{r}-2)(\tilde{r}+1)^2+6\tilde{r}\tilde{t}]\,\mathrm{erf}\left(\frac{\tilde{r}+1}{2\sqrt{\tilde{t}}}\right) \\
& + 2\sqrt{(\tilde{t}-\tilde{t}_0)/\pi}\,\exp\left[-\frac{(\tilde{r}-1)^2}{4(\tilde{t}-\tilde{t}_0)}\right][(\tilde{r}-1)(\tilde{r}+2)+4(\tilde{t}-\tilde{t}_0)] \\
& - 2\sqrt{(\tilde{t}-\tilde{t}_0)/\pi}\,\exp\left[-\frac{(\tilde{r}+1)^2}{4(\tilde{t}-\tilde{t}_0)}\right][(\tilde{r}-2)(\tilde{r}+1)+4(\tilde{t}-\tilde{t}_0)] \\
& + [(\tilde{r}-1)^2(\tilde{r}+2)+6\tilde{r}(\tilde{t}-\tilde{t}_0)]\,\mathrm{erf}\left(\frac{\tilde{r}-1}{2\sqrt{\tilde{t}-\tilde{t}_0}}\right) \\
& - [(\tilde{r}-2)(\tilde{r}+1)^2+6\tilde{r}(\tilde{t}-\tilde{t}_0)]\,\mathrm{erf}\left(\frac{\tilde{r}+1}{2\sqrt{\tilde{t}-\tilde{t}_0}}\right)\Bigg\}
\end{aligned}
\tag{17}
$$

Given parameters for external heating, i.e., $\tilde{Q}_m$ and $\tilde{t}_0$, the temporal variation of non-dimensional temperature profile before thermal runaway can be described by equations (15)-(17).

Figure 3 plots the variation of non-dimensional temperature distribution caused by the constant and uniform heating within the spherical domain of unit normalized radius. The temperature at the center, denoted by θ_{center}, is the highest. During the heating period, i.e., $\tilde{t}/\tilde{t}_0 \leq 1$, θ_{center} is shown to grow rapidly, and the high temperature regime spreads beyond $\tilde{r} > 1$, indicating that the thermal energy is continuously transferred to the surrounding mixture via heat conduction. Subsequent to the end of external heating, i.e., $\tilde{t} \geq \tilde{t}_0$, θ_{center} falls significantly and becomes comparable with the ambient temperature at $\tilde{t}/\tilde{t}_0 = 2.0$ (note that the time is normalized by the characteristic time of heat conduction, R_0^2/α). After external heating, the large temperature gradient concentrated in the heating domain with $\tilde{r} < 1$ is almost simultaneously eliminated by heat conduction, resulting in the rapid fall of central temperature as shown in figure 3.

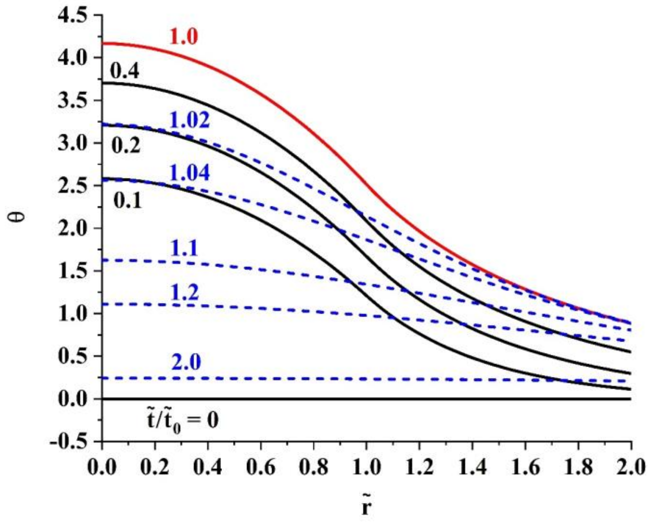

Figure 3 The temporal evolution of non-dimensional temperature distribution during (solid lines for $\tilde{t}/\tilde{t}_0 \leq 1$) and after (dashed lines for $\tilde{t}/\tilde{t}_0 > 1$) external heating within $\tilde{r} \leq 1$. The non-dimensional heating power density and heating duration are $\tilde{Q}_m = 10$ and $\tilde{t}_0 = 5$, respectively. Chemical reaction is absent in the whole process.

According to equation (1), the reaction rate rises exponentially with temperature. Therefore, ignition occurs first at $\tilde{r} = 0$, where the temperature is the highest. The transient variation of central temperature can be obtained by setting $\tilde{r} = 0$ in equations (15) and (17), which yields

For $\tilde{t} < \tilde{t}_0$

$$\theta_{center} = \frac{\tilde{Q}_m}{2}\left[1 - 2\sqrt{\tilde{t}/\pi}\exp(-1/4\tilde{t}) - (1 - 2\tilde{t})\operatorname{erf}\left(1/2\sqrt{\tilde{t}}\right)\right] \tag{18}$$

For $\tilde{t} > \tilde{t}_0$

$$\begin{aligned}\theta_{center} = \frac{\tilde{Q}_m}{2}\Big\{&2\sqrt{(\tilde{t} - \tilde{t}_0)/\pi}\exp[-1/4(\tilde{t} - \tilde{t}_0)] - 2\sqrt{\tilde{t}/\pi}\exp(-1/4\tilde{t}) \\ &+ [1 - 2(\tilde{t} - \tilde{t}_0)]\operatorname{erf}\left(1/2\sqrt{\tilde{t} - \tilde{t}_0}\right) - (1 - 2\tilde{t})\operatorname{erf}\left(1/2\sqrt{\tilde{t}}\right)\Big\}\end{aligned} \tag{19}$$

The transient variation of central temperature at various heating schemes are shown in figure 4. At the initial instant of external heating with $\tilde{t} \ll 1$, equation (18) can be expanded in series of $\tilde{t}$ close to $\tilde{t} = 0$, and it is simplified to

$$\theta_{center} \approx \tilde{Q}_m\tilde{t} \tag{20}$$

which indicates that the central temperature grows almost linearly with time, and that its increase rate is equal to the heating power density.

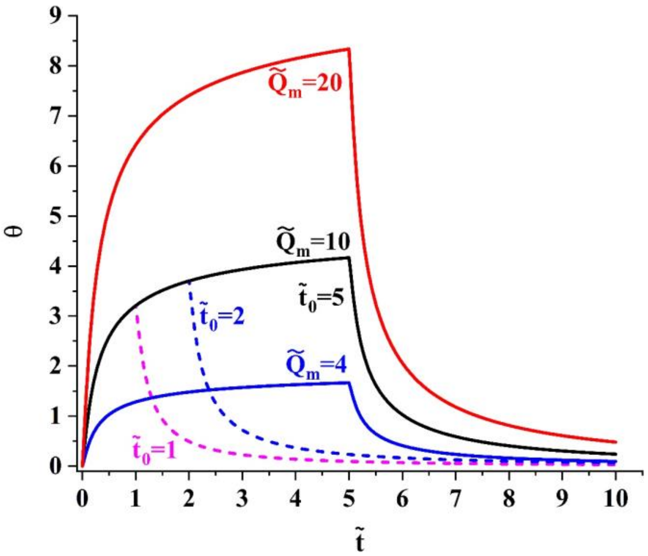

Figure 4 The transient variation of central temperature at various heating schemes characterized by $\tilde{Q}_m$ and $\tilde{t}_0$. Solid lines: same $\tilde{t}_0 = 5$ but different $\tilde{Q}_m = 4, 10$ and 20; dashed lines: same $\tilde{Q}_m = 10$ but different $\tilde{t}_0 = 1, 2$ and 5.

Approaching the end of heating stage, the central temperature tends to be saturated, whose magnitude, denoted by $\theta_{center,0}$, can be evaluated by setting $\tilde{t} = \tilde{t}_0$ in equation (18), i.e.,

$$\theta_{center,0} = \frac{1}{2}\tilde{Q}_m\left[1 - 2\sqrt{\frac{\tilde{t}_0}{\pi}}\exp\left(-\frac{1}{4\tilde{t}_0}\right) + (2\tilde{t}_0 - 1)\,\mathrm{erf}\left(\frac{1}{2\sqrt{\tilde{t}_0}}\right)\right] \tag{21}$$

Given heating duration, $\tilde{t}_0$, equation (21) indicates that saturated central temperature is linearly proportional to the heating power density, $\tilde{Q}_m$. Fixing $\tilde{Q}_m$, the central temperature keeps growing with heating duration because of continuous thermal energy input. For sufficiently long heating duration, the central temperature is bounded from above, which can be estimated by expanding equation (21) in series of $\tilde{t}_0$ as $\tilde{t}_0 \to \infty$, yielding $\theta_{center,0} \to \tilde{Q}_m/2$. It can be understood as the dynamic balance between thermal energy addition from external heating and conductive heat loss.

Figure 4 shows that the central temperature falls after switching off the external heating source. The rate can be evaluated by expanding equation (19) in series of $\tilde{t}$ close to $\tilde{t} = \tilde{t}_0$ and retaining the leading and first-order terms, i.e.,

$$\theta_{center} \approx \theta_{center,0} + \tilde{Q}_m\left[-1 - \frac{1}{\sqrt{\pi\tilde{t}_0}}\exp\left(-\frac{1}{4\tilde{t}_0}\right) + \mathrm{erf}\left(\frac{1}{2\sqrt{\tilde{t}_0}}\right)\right](\tilde{t} - \tilde{t}_0) \tag{22}$$

The above equation indicates that the temperature decrease rate is also proportional to the heating power density, i.e., $d\theta_{center}/d\tilde{t} \approx \tilde{Q}_m$. This is reasonable since higher heating power density creates larger temperature gradient at the center of heating domain and thus leads to stronger conductive heat loss.

3.2 Thermal runaway at the heating center

The normalized temperature is described by equations (15) – (17). Since the rate of chemical reaction increases exponentially with temperature according to equation (1), the temperature rise caused by external heating can initiate thermal runaway with an appropriate time lapse, denoted by $\tilde{t}_{explosion}$. The thermal runaway first occurs at the center, $\tilde{r} = 0$, where the highest temperature appears (see figure 3). The central temperature grows according to equations (18) and (19). The reactivity at the center exhibits historical effect and must be taken into account to evaluate the time delay of thermal runaway. In terms of suitably defined reaction progress variable, an estimation of $\tilde{t}_{explosion}$ can be determined by the Livengood-Wu integral [35-37]:

$$1 = \int_0^{\tilde{t}_{explosion}} \frac{1}{\tilde{t}_{ch}} dt' \qquad (23)$$

where the chemical reaction time scale $\tilde{t}_{ch}$ is the ignition delay time for a homogeneous system with initial temperature equal to θ_{center}.

The autoignition first occurs in an infinitesimal spherical domain of radius $\tilde{r}_{runaway}$ close to the heating center, which is exceedingly smaller than the heating domain, i.e., $\tilde{r}_{runaway} \ll 1$. The overall heat loss from the autoignition domain is characterized by the temperature gradient at the outer edge. Due to symmetry, this temperature gradient exhibits to be vanishingly small, and accordingly we may assume that the thermal runaway there takes place adiabatically. The ignition process in an adiabatic homogeneous system can be described by transient variation of temperature resulting from heat accumulation. In terms of the scaled temperature, defined by $\hat{\theta} = (\theta + 1)/\tilde{q}$ where $\tilde{q}$ is the normalized heat of reaction defined in equation (9), the energy equation can be written as

$$\frac{d\hat{\theta}}{d\tilde{t}} = \tilde{B} e^{-\hat{\theta}_a/\hat{\theta}} \qquad (24)$$

Before thermal runaway occurs, the reactant consumption tends to be negligible, suggesting minor effects of mass diffusion. Therefore, the mass fraction Y does not appear explicitly in the reaction rate term in equation (24).

To investigate the temperature rise that characterizes the process of thermal runaway, it is conventional to define a small quantity in terms of activation temperature [38]:

$$\epsilon = \hat{\theta}^2/\hat{\theta}_a \ll 1 \tag{25}$$

The scaled temperature $\hat{\theta}$ is then expanded as asymptotic series in terms of ϵ, giving

$$\hat{\theta} = \hat{\theta}_{center} + \epsilon\chi \tag{26}$$

where $\hat{\theta}_{center}$ is the initial temperature of the homogeneous system, and $\epsilon\chi$ represents temperature rise due to chemical reaction. Substituting the expansion (26) into equation (24), one obtains the equation for temperature perturbation χ

$$\frac{d\chi}{d\tilde{t}} = \frac{\tilde{B}e^{-\hat{\theta}_a/\hat{\theta}_{center}}}{\epsilon}e^{\chi} \tag{27}$$

The solution of equation (27) subject to initial condition $\chi = 0$ at $\tilde{t} = 0$ is

$$\chi = -\ln\left(1 - \tilde{t}\,\tilde{B}e^{-\hat{\theta}_a/\hat{\theta}_{center}}/\epsilon\right) \tag{28}$$

Equation (28) indicates that as $\tilde{t} \to \epsilon e^{\hat{\theta}_a/\hat{\theta}_{center}}/\tilde{B}$, χ becomes infinitely large, suggesting the occurrence of thermal runaway. Therefore, the ignition delay time is $\tilde{t}_{ch} = \epsilon e^{\hat{\theta}_a/\hat{\theta}_{center}}/\tilde{B}$. In terms of non-dimensional temperature θ, it can be written as

$$\tilde{t}_{ch} = \frac{(1+\theta_{center})^2 e^{(1+\theta_a)/(1+\theta_{center})}}{(1+\theta_a)\tilde{q}\tilde{B}} \tag{29}$$

Substituting the transient variation of central temperature given by equations (18) and (19) into equation (29), the variation of $\tilde{t}_{ch}$ with time can be determined. Evaluating the integral on the right-hand side of (23), the delay time for thermal runaway, $\tilde{t}_{explosion}$ can be evaluated.

Due to complicated dependence of θ_{center} upon $\tilde{t}$, the explicit expression for $\tilde{t}_{explosion}$ cannot be obtained. Nevertheless, at large heating power density, the central temperature rises exceedingly rapidly, which, according to equations (29) and (23), leads to significant reduction of delay time of thermal runaway. In such situations, we may suppose that the delay time of thermal runaway would be much shorter than the heating duration, i.e., $\tilde{t}_{explosion} \ll \tilde{t}_0$. According to equation (20), the central temperature grows almost linearly with the time at the initial stage. This enables us to evaluate the Livengood-Wu integral analytically. Consequently, an explicit form for $\tilde{t}_{explosion}$ is obtained:

$$\tilde{t}_{explosion} = \frac{1+\theta_a}{\tilde{Q}_m \ln\left(\tilde{B}\tilde{q}/\tilde{Q}_m\right)} \tag{30}$$

In most situations, we have $\tilde{B}\tilde{q} \gg \tilde{Q}_m$. Therefore equation (30) indicates that $\tilde{t}_{explosion}$ increases when $\tilde{Q}_m$ decreases.

At relatively low heating power density, thermal runaway tends to take place at the end of heating duration, when the central temperature approaches to the saturated value. Because of rapid fall of central temperature subsequent to the end of heating duration, thermal runaway can hardly appear for $\tilde{t} > \tilde{t}_0$. Consequently, we can define the critical condition for thermal runaway by equating $\tilde{t}_{explosion}$ to the heating duration $\tilde{t}_0$, i.e., thermal runaway occurs at the very instant of removing the external heating source and $\tilde{t}_{explosion} = \tilde{t}_0$. Substituting equation (29) into equation (23) yields the following expression for the critical condition:

$$\int_0^{\tilde{t}_0} \frac{e^{-(1+\theta_a)/(1+\theta_{center})}}{(1+\theta_{center})^2} d\tilde{t}' = \frac{1}{(1+\theta_a)\tilde{q}\tilde{B}} \tag{31}$$

where the central temperature θ_{center} is given by equation (18). Equation (31) determines the critical heating power density, denoted by $\tilde{Q}_{cr}$, for given heating duration $\tilde{t}_0$.

To calculate $\tilde{t}_{explosion}$, the parameters related to one-step chemistry model, i.e., the activation temperature θ_a, heat of reaction $\tilde{q}$, and reaction frequency factor $\tilde{B}$, must be specified. We choose the stoichiometric CH$_4$/air mixture as the representative reactant. The values of $B = 9.5 \times 10^8$ s^{-1} and $T_a = 25000$ K are obtained by fitting the homogeneous ignition delay time calculated from simulation using detailed chemistry based on equation (29). The heat of reaction $\tilde{q}$ is equivalent to the non-dimensional adiabatic flame temperature because of energy conservation, i.e., $q = \rho c_p(T_{ad} - T_\infty)$, which divided by $\rho c_p T_\infty$ gives $\tilde{q} = \theta_{ad}$. To evaluate the thermal and transport properties, such as density ρ, heat capacity c_p, and thermal conductivity λ, which change with temperature, it requires a reference temperature, denoted by T_{ref}. The reference temperature can be suitably defined as the "average" temperature during the thermal runaway process. Usually, the temperature at the instant of thermal runaway is comparable with the adiabatic flame temperature. For convenience in calculation, we set $T_{ref} = 1800$K. Based on test calculation, we find that varying T_{ref} can hardly alter the general features of various theoretically predicted results though quantitative change exists.

Figure 5 shows that delay time for thermal runaway decreases monotonically with the heating power density. Setting $\tilde{t}_{explosion}$ equal to $\tilde{t}_0$, the corresponding $\tilde{Q}_m$ read in abscissa of figure 5 determines the critical heating power density, $\tilde{Q}_{cr}$, below which thermal runaway cannot be observed in the reactant. Figure 5 shows that at large heating power density with $\tilde{Q}_m > 40$, equation (30) accurately predicts

$\tilde{t}_{explosion}$. This indicates that heating duration can be made arbitrarily short at sufficiently high heating power density. This ideal phenomenon may not take place in actual ignition problem because exceedingly high $\tilde{Q}_m$ induces strong thermal expansion and generates a shock wave. In addition to heat conduction, the heat loss caused by thermal expansion is significant and thereby leads to a longer delay time for thermal runaway. In particular, there exists a lower bound for $\tilde{Q}_{cr}$ which corresponds to $\tilde{t}_0 \to \infty$, i.e., thermal runaway never occurs. This minimum critical heating power density for thermal runaway, denoted by $\tilde{Q}_{cr,runaway}$, can be evaluated implicitly by setting $\tilde{t}_0$ in equation (31) to be infinity and is depicted in figure 5.

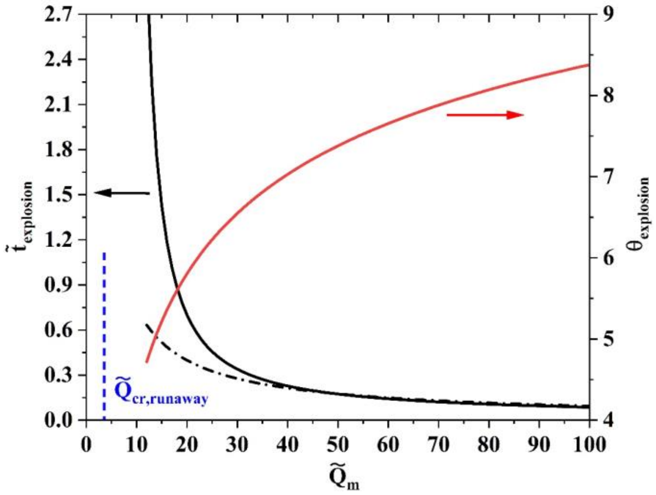

Figure 5 Change of time for thermal runaway, $\tilde{t}_{explosion}$, and the corresponding central temperature at that instant with external heating power density $\tilde{Q}_m$. The dash-dot line represents the $\tilde{t}_{explosion}$ based on equation (30).

Knowing the delay time for thermal runaway, the total thermal energy deposition in this process can be evaluated. In non-dimensional form, we have

$$\tilde{E}_{explosion} = \tilde{Q}_m \tilde{t}_{explosion} \tag{32}$$

where $\tilde{E}_{explosion} = E_{explosion}/\left(4\pi R_0^3 \rho c_p T_\infty/3\right)$. At given heating power density $\tilde{Q}_m$, we may consider $\tilde{E}_{explosion}$ as the critical ignition energy, below which thermal runaway cannot occur. Figure 6 shows that the $\tilde{E}_{explosion}$ varies nonmonotonically with $\tilde{Q}_m$. As $\tilde{Q}_m$ approaches to $\tilde{Q}_{cr,runaway}$, as indicated by the blue dashed line in figure 6, the critical ignition energy increases abruptly, indicating that ignition becomes extremely difficult.

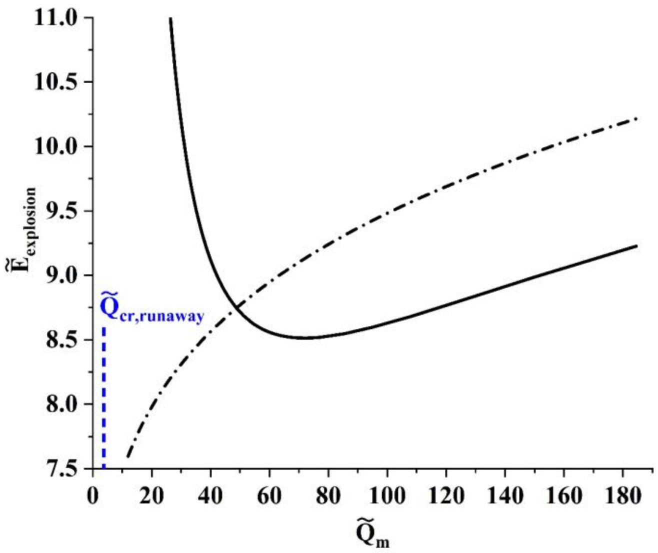

Figure 6 Change of critical ignition energy with heating power density. The dash-dot line represents the $\tilde{E}_{explosion}$ based on equation (33).

At relatively large $\tilde{Q}_m$, the critical ignition energy tends to increase with heating power density. Since analytical expression for $\tilde{t}_{explosion}$ is available in equation (30), the critical ignition energy can be written explicitly in terms of heating power density, i.e.,

$$\tilde{E}_{explosion} = \frac{(1+\theta_a)}{\ln\left(\tilde{B}\theta_{ad}/\tilde{Q}_m\right)} \tag{33}$$

Equation (33) shows $\tilde{E}_{explosion}$ increases slightly with $\tilde{Q}_m$. The results based on equation (33) is plotted in figure 6 and there is around 10% over-prediction for $\tilde{Q}_m > 50$.

The nonmonotonic variation of critical ignition energy suggests that there exists an optimized heating power density, which corresponds to the lowest $\tilde{E}_{explosion}$ during the thermal runaway process. Since both ignition energy and heating power density presented in figure 6 are in non-dimensional form, the optimized heating power density, around $\tilde{Q}_m = 70$, can be generalized to various ignition systems.

3.3 Flame kernel emergence

According to Vázquez-Espí and Liñán [7], intensive chemical reaction subsequent to thermal runaway occurs within a small region in the central heating domain, which is known as the Frank-Kamenetskii region (abbreviated for FK region hereinafter). The temperature drop within the FK region is of order

$O(\epsilon)$, where ϵ is evaluated by equation (25) in terms of the central temperature at the instant of thermal runaway, denoted by $\theta_{explosion}$, i.e., $\theta_{explosion} = \theta_{center}\left(\tilde{t}_{explosion}\right)$.

The temperature at the edge of FK region, denoted by θ_{FK}, deviates slightly from $\theta_{explosion}$ at the center of heating domain, i.e., $\theta_{FK} = (1-\epsilon)\theta_{explosion}$. Accordingly, the radius of the FK region, $\tilde{r}_{FK}$, can be determined by $\theta(\tilde{r}_{FK}) = \theta_{FK}$. Figure 3 indicates that the temperature at the edge of heating domain, denoted by $\theta_{edge} = \theta(\tilde{r}=1)$, tends to be considerably lower than θ_{center}. This indicates that the radius of Frank-Kamenetskii region satisfies that $\tilde{r}_{FK} \ll 1$. Therefore, we have the following approximation for θ_{FK} at the instant of thermal runaway:

$$\theta_{FK} = \theta_{explosion} + \frac{1}{2}\left(\frac{\partial^2\theta}{\partial\tilde{r}^2}\right)_{\tilde{r}=0} \tilde{r}_{FK}^2 \tag{34}$$

Solving equation (34) for $\tilde{r}_{FK}$ and using $\theta_{FK} = (1-\epsilon)\theta_{explosion}$ and equation (25) for ϵ, we obtain

$$\tilde{r}_{FK} = \sqrt{\frac{2\theta_{explosion}\left(\theta_{explosion}+1\right)^2}{(\theta_a+1)\tilde{q}(-\partial^2\theta/\partial\tilde{r}^2)_{\tilde{r}=0}}} \tag{35}$$

where the second order derivative is derived from equation (15), i.e.,

$$-\left(\frac{\partial^2\theta}{\partial\tilde{r}^2}\right)_{\tilde{r}=0} = \frac{\tilde{Q}_m}{6}\left[1 + \frac{1}{\sqrt{\pi\tilde{t}_{explosion}}}\exp\left(-\frac{1}{4\tilde{t}_{explosion}}\right) - \operatorname{erf}\left(\frac{1}{2\sqrt{\tilde{t}_{explosion}}}\right)\right] \tag{36}$$

Since thermal runaway initiates intensive chemical reaction, the reactant consumption becomes considerable, which is associated with additional heat release at the center. According to Vázquez-Espí and Liñán [7], an order of $O(\epsilon)$ temperature drop leads to an order of $O(1)$ reduction in chemical reaction rate. Therefore, the chemical reaction outside the FK region is insignificant. During the consumption of reactant in the FK region, the thermal energy budget involves external heating, chemical heat release, and conductive heat loss to the surroundings. Therefore, the governing equations are of general form given by equations (8) and (9), for which analytical solutions cannot be obtained.

The appearance of reaction front is characterized by complete consumption of reactant, which generates an interface separating the burnt and unburnt regions. Since the temperature within the FK region is not uniform, the chemical reaction rate varies from the center to the edge of FK region. Here we are interested in evaluating the time scale for reactant depletion at the center, where the chemical reaction is most vigorous. We may tackle the problem from a practical perspective. Integrating the governing equations (8) and (9) yields

$$\frac{d\overline{\theta}}{d\tilde{t}} = \frac{4\pi\tilde{r}_{FK}^2}{\tilde{V}_{FK}}\left(\frac{\partial\theta}{\partial\tilde{r}}\right)_{\tilde{r}=\tilde{r}_{FK}} + \tilde{Q}_m + \frac{4\pi\tilde{q}\tilde{B}}{\tilde{V}_{FK}}\int_0^{\tilde{r}_{FK}} Y\exp\left(-\frac{\theta_a+1}{\theta+1}\right)\tilde{r}^2 d\tilde{r} \tag{37}$$

$$\frac{d\overline{Y}}{d\tilde{t}} = \frac{1}{Le}\frac{4\pi\tilde{r}_{FK}^2}{\tilde{V}_{FK}}\left(\frac{\partial Y}{\partial\tilde{r}}\right)_{\tilde{r}=\tilde{r}_{FK}} - \frac{4\pi\tilde{B}}{\tilde{V}_{FK}}\int_0^{\tilde{r}_{FK}} Y\exp\left(-\frac{\theta_a+1}{\theta+1}\right)\tilde{r}^2 d\tilde{r} \tag{38}$$

where $\tilde{V}_{FK} = 4\pi\tilde{r}_{FK}^3/3$ is the volume of the FK region. The average temperature and mass fraction of reactant in the FK region are defined by

$$\overline{\theta} = \frac{4\pi}{\tilde{V}_{FK}}\int_0^{\tilde{r}_{FK}} \theta\tilde{r}^2 d\tilde{r}\,, \qquad \overline{Y} = \frac{4\pi}{\tilde{V}_{FK}}\int_0^{\tilde{r}_{FK}} Y\tilde{r}^2 d\tilde{r} \tag{39}$$

After integration, equations (8) and (9) are converted to ordinary differential equations (37) and (38) for average temperature and mass fraction of reactant. The terms on the right-hand sides of equations (37) and (38) could be evaluated if the profiles of temperature and reactant mass fraction in the FK region are known. Since the FK-region is small, $\tilde{r}_{FK} \ll 1$, we can assume that the temperature profile inside the FK region is

$$\theta = \theta_{center} - (\theta_{center} - \theta_{FK})\frac{\tilde{r}^2}{\tilde{r}_{FK}^2} \tag{40}$$

It is the simplest mathematical form of temperature profile that satisfies the symmetry condition at the center, i.e., $(d\theta/d\tilde{r})_{\tilde{r}=0} = 0$, and $\theta_{center} = \theta_{FK}$ at the edge of the FK region. It is noted that, the θ_{center} appearing in equation (40) differs from that in equation (18) because of additional heat release from chemical reaction and thus remains to be determined by solving equation (37). However, the temperature at the edge of FK region, θ_{FK}, due to negligible chemical reaction, can be determined via equation (15) at $\tilde{r} = \tilde{r}_{FK}$, and thereby can be considered as known function of time. From equation (40) we have

$$\left(\frac{\partial\theta}{\partial\tilde{r}}\right)_{\tilde{r}=\tilde{r}_{FK}} = -\frac{2(\theta_{center} - \theta_{FK})}{\tilde{r}_{FK}} \tag{41}$$

To evaluate the integrals of chemical reaction in equations (37) and (38), we also need the profile of reactant mass fraction in the FK region. At the center, the gradient of Y must be zero due to symmetry. Outside the FK region, the consumption of reactant is negligible, i.e., $Y(\tilde{r} > \tilde{r}_{FK}) = 1$. Because of comparably high temperature, the subsequent chemical reaction rate is substantially facilitated. Accordingly, the consumption rate of reactant at the center of the FK region is significantly faster than the supply rate by diffusion from the surrounding. It demonstrates that the chemical reaction at the heating center dominates the generation of reaction front, which can hardly be affected by mass diffusion. Therefore, it introduces an additional condition that the gradient of reactant mass fraction should vanish at the edge of the FK region, i.e., $(\partial Y/\partial\tilde{r})_{\tilde{r}=\tilde{r}_{FK}} = 0$. In analogy to temperature profile given by equation (40), the mass fraction distribution can be constituted based on the conditions given above. The simplest mathematical form appears to be a cubic function of $\tilde{r}$, given by

$$Y = Y_{center} + 3(1 - Y_{center})\frac{\tilde{r}^2}{\tilde{r}_{FK}^2} - 2(1 - Y_{center})\frac{\tilde{r}^3}{\tilde{r}_{FK}^3} \tag{42}$$

where Y_{center} refers to the reactant mass fraction at the center of the FK region, which falls in the course of time due to chemical reaction.

With help of the above constituted temperature and mass fraction profiles in the FK region, given by equations (40) and (42), respectively, the last term on the right-hand side of equation (37) becomes

$$\frac{4\pi\tilde{q}\tilde{B}}{\tilde{V}_{FK}}\int_0^{\tilde{r}_{FK}} Y\exp\left(-\frac{\theta_a + 1}{\theta + 1}\right)\tilde{r}^2 d\tilde{r} = \tilde{q}\tilde{B}\exp\left(-\frac{\theta_a + 1}{\theta_{center} + 1}\right)F(\theta_{center}, Y_{center}) \tag{43}$$

where

$$\begin{aligned} F(\theta, Y) = &-\frac{3(1+\theta)^2}{2(\theta_a + 1)(\theta - \theta_{FK})}\exp\left[-\frac{(\theta_a + 1)(\theta - \theta_{FK})}{(1+\theta)^2}\right] \\ &+\frac{3c\sqrt{\pi}(1+\theta)^3}{4(\theta_a + 1)^{3/2}(\theta - \theta_{FK})^{3/2}}\operatorname{erf}\left[\frac{\sqrt{(\theta_a + 1)(\theta - \theta_{FK})}}{1+\theta}\right] \\ &-\frac{3(1-Y)(1+\theta)^4}{4(\theta_a + 1)^2(\theta - \theta_{FK})^2}\exp\left[-\frac{(\theta_a + 1)(\theta - \theta_{FK})}{(1+\theta)^2}\right] \\ &+\frac{27(1-Y)\sqrt{\pi}(1+\theta)^5}{8(\theta_a + 1)^{5/2}(\theta - \theta_{FK})^{5/2}}\operatorname{erf}\left[\frac{\sqrt{(\theta_a + 1)(\theta - \theta_{FK})}}{1+\theta}\right] \\ &-\frac{6(1-Y)(1+\theta)^6}{(\theta_a + 1)^3(\theta - \theta_{FK})^3}\left\{1 - \exp\left[-\frac{(\theta_a + 1)(\theta - \theta_{FK})}{(1+\theta)^2}\right]\right\} \end{aligned} \tag{44}$$

Substituting equations (40) and (42) into equation (39) yields the average temperature and mass fraction in the FK region:

$$\overline{\theta} = \frac{1}{5}(2\theta_{center} + 3\theta_{FK}), \qquad \overline{Y} = \frac{1}{5}(4 + Y_{center}) \tag{45}$$

Since chemical reaction rate at the edge of the FK region is significantly lower than that at the center, we may assume that the rate of change in θ_{FK} is negligible compared to that of θ_{center}. Therefore, we have

$$\frac{d\overline{\theta}}{d\tilde{t}} \approx \frac{2}{5}\frac{d\theta_{center}}{d\tilde{t}}, \qquad \frac{d\overline{Y}}{d\tilde{t}} \approx \frac{1}{5}\frac{dY_{center}}{d\tilde{t}} \tag{46}$$

Substituting equations (41), (43), and (46) into equations (37) and (38), we obtain the following ordinary differential equations that describe the variation of central temperature and reactant mass fraction during the stage of reaction front setup:

$$\frac{d\theta_{center}}{d\tilde{t}} = -\frac{15(\theta_{center} - \theta_{FK})}{\tilde{r}_{FK}^{2}} + \frac{5}{2}\tilde{Q}_m + \frac{5}{2}\tilde{q}\tilde{B}\exp\left(-\frac{\theta_a + 1}{\theta_{center} + 1}\right)F(\theta_{center}, Y_{center}) \tag{47}$$

$$\frac{dY_{center}}{d\tilde{t}} = -5\tilde{B}\exp\left(-\frac{\theta_a + 1}{\theta_{center} + 1}\right)F(\theta_{center}, Y_{center}) \tag{48}$$

Since the function $F(\theta, Y)$ given by equation (44) is nonlinear, equations (47) and (48) must be solved numerically.

Figure 7 shows the transient variation of temperature and reactant mass fraction at the center of the FK region after the thermal runaway occurs. The delay time for thermal runaway, according to equation (23), is $\tilde{t}_{explosion} = 0.4$. As chemical reaction is initiated for $\tilde{t} > \tilde{t}_{explosion}$, the reactant is converted into product, leading to the drop of $\tilde{Y}_{center}$. The growth of θ_{center} results from the competition among chemical heat generation, external heating and conductive heat loss to the surroundings.

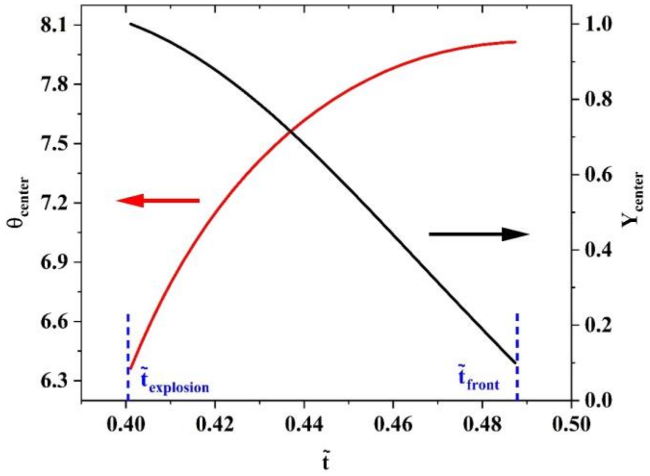

Figure 7 Transient variation of temperature and reactant mass fraction at the center of the FK region during the establishment of reactant front. The non-dimensional heating power density is $\tilde{Q}_m = 27$ and heating duration is $\tilde{t}_0 = 5$.

The setup of reaction front is characterized by the complete consumption of reactant, which tends to be infinitely long because of the long tail exponential decay of Y. For practical consideration, the end of reactant consumption can be measured by a threshold value of mass fraction, denoted by Y_{end}, which is set to be 0.1. Based on the evolution of Y_{center} obtained numerically from equations (47) and (48), we can determine the delay time for the depletion of reactant at the center $\tilde{t}_{consumption}$ by

$$Y\left(\tilde{t}_{consumption}\right) = 0.1 \tag{49}$$

Accordingly, the temperature at the reaction front, denoted by θ_{front}, is calculated by

$$\theta_{front} = \theta_{center}\left(\tilde{t}_{consumption}\right) \tag{50}$$

Knowing $\tilde{t}_{explosion}$ and $\tilde{t}_{consumption}$ given by equations (30) and (49) respectively, the time lapse for establishing the reaction front at the center of heating domain is accordingly determined as their sum, i.e., $\tilde{t}_{front} = \tilde{t}_{explosion} + \tilde{t}_{consumption}$, as depicted in figure 1.

For the representative situation of $\tilde{Q}_m = 27$ and $\tilde{t}_0 = 5$, figure 7 shows that $\tilde{t}_{front} = 0.49$, which is slightly longer than $\tilde{t}_{explosion} = 0.40$. This indicates that $\tilde{t}_{consumption}/\tilde{t}_{front} \ll 1$, i.e., the stage of reactant consumption occurs more readily than the thermal runaway at the center of heating domain. Such short duration can be attributed to the self-accelerating behavior of chemical reaction with temperature growth. It also verifies our previous assumptions that the diffusion of reactant from the surroundings and transient variation of temperature at the edge of FK region are both negligible during the reactant consumption at the center of heating domain.

Approaching $\tilde{t}_{front}$, the growth rate of θ_{center} rapidly falls. Phenomenologically, there exists a saturated value for θ_{center}, which can be understood from two aspects. On one hand, the reduction of reactant mass fraction lowers the reaction rate and chemical heat release rate. On the other hand, the increase of central temperature enhances the heat loss rate by thermal conduction, which is represented by the first term on the right-hand side of equation (47) and is linearly proportional to θ_{center}.

Figure 8 shows the change of temperature profile in the FK region at different instants. The initial temperature is uniformly equal to that in the environment. Before thermal runaway, the temperature profiles are determined by the analytical solution (15) and are indicated by the blue lines in figure 8. The period is evenly divided with equal time $\Delta = 0.2\tilde{t}_{explosion}$. Since the heating power density is uniform, the temperature profile in the FK region tends to be flat. Slight temperature gradient arises because of geometric symmetry at the center. At the onset of thermal runaway, the heat release and reactant consumption by reaction must be taken into account, and therefore analytical solutions for (8) and (9) become unavailable. Instead, the temporal variation of the temperature and reactant mass fraction in the FK region can be solved from equations (37) and (38), which are obtained by integrating equations (8) and (9) with knowledge of given temperature and mass fraction profiles in the FK region. During the stage of reactant consumption, i.e., $\tilde{t} > \tilde{t}_{explosion}$, the temporal variation of temperature and reactant mass fraction at the heating center $\theta_{center}(\tilde{t})$ and $Y_{center}(\tilde{t})$ are determined by equations (47) and (48), respectively. In addition, the nondimensional temperature at the edge of FK region $\theta_{FK}(\tilde{t})$ can be obtained by evaluating equation (15) at $\tilde{r} = \tilde{r}_{FK}$. Substituting the solutions for θ_{center} and Y_{center} and θ_{FK} into the constituted relations (40) and (42), the temperature and mass fraction profiles within the FK region during the establishment of flame front are determined, which are plotted as red solid lines in figure 8 and black solid lines in figure 9 respectively.

It is seen that θ_{center} tends to grow more rapidly that θ_{FK} because of additional heat release provided by chemical reaction. Consequently, the temperature gradient in the FK region becomes increasingly noticeable, which increases the conductive heat loss to the surroundings and leads to the saturation of the central temperature.

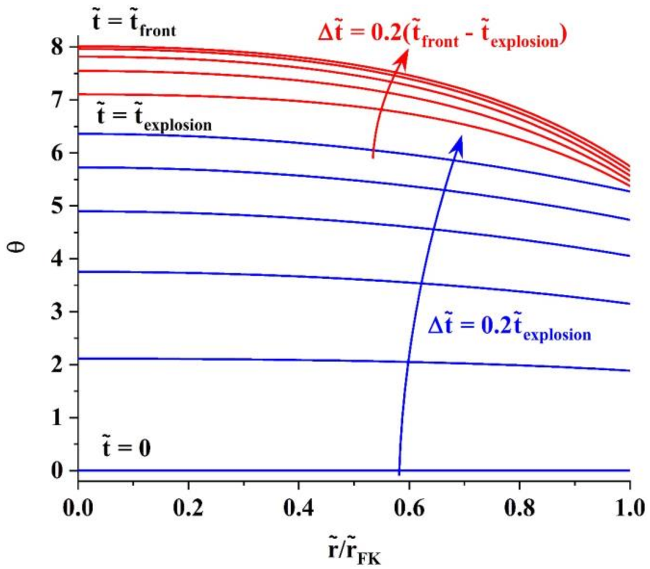

Figure 8 The transient variation of temperature profile in the FK region. The non-dimensional heating power density is $\tilde{Q}_m = 27$ and heating duration is $\tilde{t}_0 = 5$.

Figure 9 shows the transient variation of reactant mass fraction in the FK region after thermal runaway is initiated, i.e., $\tilde{t} = \tilde{t}_{explosion}$. The profile of Y falls concavely as Y_{center} reduces, and magnitude of $dY/d\tilde{r}$ in average reaches $O(1)$ when the reaction front is almost setup. This indicates that the gradient of reactant mass fraction in the FK region tends to be substantially smaller than that of temperature during the reaction front formation. The supply of fresh reactant by diffusion tends to be insignificant during the reaction front formation at the center of heating domain. The drop of Y_{center} is primarily due to chemical reaction, which is consistent with the mathematical form of equation (38). By consistency we mean that the characteristic time scale for flame front generation at the center of heating domain is much shorter than the diffusion time scale, which is proportional to the conduction time scale by a factor of 1/Le. Therefore, it verifies the assumption of neglecting the diffusion term in equation (38). The consistent results for profiles of temperature and reactant mass fraction in the FK region implies the plausibility of the constituted profiles for θ and Y, given by equations (40) and (42), respectively.

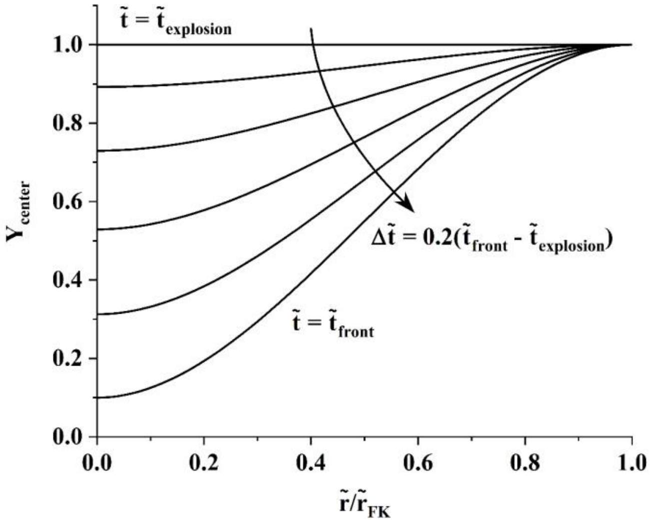

Figure 9 The transient variation of reactant mass fraction in the FK region. The non-dimensional heating power density is $\tilde{Q}_m = 27$ and heating duration is $\tilde{t}_0 = 5$.

Nevertheless, the appearance of conduction term in equation (37) shall be understood from an alternative perspective. The combining effect of external heating and chemical heat release results in considerable growth of temperature at the center. The comparably large temperature gradient greatly intensifies the heat loss from the FK region. Therefore, the conductive term must be retained in the energy equation (37).

Figure 10 shows that $\tilde{t}_{front}$ decreases with $\tilde{Q}_m$, indicating that the reaction front can be more readily established for stronger external heating. This can be understood as follows. As shown in figure 5, for larger $\tilde{Q}_m$, the delay time for thermal runaway, $\tilde{t}_{explosion}$ becomes shorter, and the central temperature at the instant of thermal runaway tends to be higher. The growth of $\theta_{explosion}$ facilitates chemical reaction and accordingly shortens the subsequent consumption time of reactant at the center. Since reactant can be more readily converted to product, the thermal energy accumulation close to the center of heating domain is facilitated, yielding a higher temperature of the reaction front.

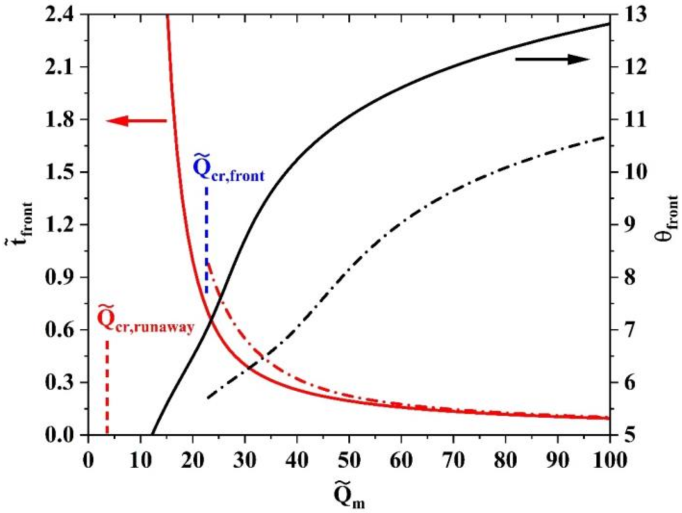

Figure 10 Change of the time lapse for the setup of reaction front, $\tilde{t}_{front}$, and the central temperature at that instant, θ_{front}, with external heating power density, $\tilde{Q}_m$. The solid lines correspond to situations in which the external heating always exists during the formation of reaction front, i.e., $\tilde{t}_0 > \tilde{t}_{front}$. The dash-dotted lines represent the particular situations that the external heating is removed at the onset of thermal runaway, i.e., $\tilde{t}_0 = \tilde{t}_{explosion}$.

Since $\theta_{explosion}$ grows with $\tilde{Q}_m$, the chemical reaction subsequent to thermal runaway is a self-sustained process when the heating power density becomes sufficiently high, i.e., the reactant at the center can still be depleted without external heating. However, in such situations, the conductive heat loss must be balanced by chemical heat release. It results in a lower accumulation rate of thermal energy, which corresponds to a longer $\tilde{t}_{front}$ and lower θ_{front}, as indicated by the dash-dot lines in figure 10.

In addition to $\tilde{Q}_{cr,explosion}$ that characterizes the minimum heating power for thermal runaway, there exists one more threshold heating power density, denoted by $\tilde{Q}_{cr,front}$, below which the reaction front cannot be formed without continued external heating after thermal runaway at the center. It could be understood that for situations with $\tilde{Q}_m < \tilde{Q}_{cr,front}$, the central temperature at $\tilde{t} = \tilde{t}_{explosion}$ is too low to induce sufficient chemical heat release to balance with the conductive heat loss. The chemical reaction initiated by thermal runaway is immediately terminated due to the removal of heating source at $\tilde{t} = \tilde{t}_{explosion}$. For $\tilde{t}_{front}$, the difference between the solid and dash-dot lines in figure 10 falls rapidly as increasing the heating power density.

3.4 Propagation of the reaction front

Depletion of reactant at the center creates a reaction front there, which propagates outwardly. Due to thermal energy addition, the reactant mixture within the heating domain is close to the state of autoignition, which provides substantial assistance to the propagation of the flame front. Accordingly, the moving speed of the flame front within the heating domain is considerably greater than the conventional spherical flame expanding in relatively cool environment. The results in figure 7 shows that the consumption time of reactant due to chemical reaction is significantly shorter than the diffusion time scale, i.e., $\tilde{t}_{consumption} \ll 1$. This indicates that the apparent motion of the reaction front from the center to the edge of heating domain should be considered as sequential setup of reaction front in the radial direction. The propagating speed of the reaction front is denoted by u_{front}, whose non-dimensional form can be written as $\tilde{u}_{front} = u_{front}R_0/\alpha$. Accordingly, based on the gradient theory by Zel'dovich [39], the propagation speed of flame front from the center to the edge of the heating domain is correlated to the spatial variation of ignition delay time, which exhibits in the following form

$$\tilde{u}_{front} = \left(\frac{\partial \tilde{t}_{front}}{\partial \tilde{r}}\right)^{-1} \tag{51}$$

Considering $\tilde{u}_{front}$ as a function of $\tilde{r}$, the time lapse for the reaction front's arrival at edge of heating domain, denoted by $\tilde{t}_{propagation}$, can be evaluated as

$$\tilde{t}_{propagation} = \int_0^1 \frac{1}{\tilde{u}_{front}} d\tilde{r}' \tag{52}$$

Substituting equation (51) into the integral on the right side and using chain rule of derivative, we have

$$\tilde{t}_{propagation} = \int_0^1 \frac{\partial \tilde{t}_{front}}{\partial \theta} \left(\frac{d\theta}{d\tilde{r}'}\right)_{\tilde{t}_{front}} d\tilde{r}' \tag{53}$$

The actual process of reaction front propagation is very complicated. Because of nonuniformity of temperature profile inside the heating domain, the time scale measuring the establishment of reactant front $\tilde{t}_{front}$ changes with radial distance from the center. However, the arrival of reaction front rapidly rises the local temperature and thereby significantly facilitates the chemical reaction nearby. This indicates that the term $\left(\partial \tilde{t}_{front}/\partial \theta\right)$ cannot be suitably evaluated based on the local temperature. Instead, we may assume that $\left(\partial \tilde{t}_{front}/\partial \theta\right)$ changes slightly with radial distance and can be calculated at the heating center for convenience. Accordingly, the expression for $\tilde{t}_{propagation}$ is simplified to

$$\tilde{t}_{propagation} \approx \left(\frac{\partial \tilde{t}_{front}}{\partial \theta}\right)_{\tilde{r}=0} \int_0^1 \left(\frac{d\theta}{d\tilde{r}'}\right)_{\tilde{t}=\tilde{t}_{front}} d\tilde{r}' \tag{54}$$

Considering the fact that $\tilde{t}_{front} = \tilde{t}_{explosion} + \tilde{t}_{consumption}$, the evaluation of $\left(\partial \tilde{t}_{front}/\partial \theta\right)_{\tilde{r}=0}$ requires an explicit expression between $\tilde{t}_{consumption}$ and θ, which cannot be obtained. Nevertheless, we acknowledge that the reaction front setup is controlled by chemical reaction rate. As temperature increases, both thermal runaway and reactant consumption become more readily to take place. In addition, it usually has $\tilde{t}_{consumption} \ll \tilde{t}_{explosion}$ because of relatively higher temperature led by external heating. Therefore, we have the following approximate relationship

$$\left(\frac{\partial \tilde{t}_{front}}{\partial \theta}\right)_{\tilde{r}=0} \approx \left(\frac{\partial \tilde{t}_{explosion}}{\partial \theta}\right)_{\tilde{r}=0} \tag{55}$$

Since $\tilde{t}_{explosion}$ is determined by the Livengood-Wu integral, the temperature dependence of the characteristic reaction time $\tilde{t}_{ch}$, given by equation (29), is not directly affected by the integration. We suppose that the dependence of $\tilde{t}_{explosion}$ and hence $\tilde{t}_{front}$ according to equation (55) can be assessed by the derivative of $\tilde{t}_{ch}$ with respect to θ. Therefore, from practical perspective, we have

$$\left(\frac{\partial \tilde{t}_{front}}{\partial \theta}\right)_{\tilde{r}=0} \approx -\frac{\theta_a - 1 - 2\theta_{front}}{\tilde{B}\tilde{q}(1+\theta_a)} e^{(1+\theta_a)/(1+\theta_{front})} \tag{56}$$

where the non-dimensional temperature at the reaction front θ_{front} is calculated by equation (50).

During reaction front propagation, reactant within the central heating domain is continuously consumed. Rigorous determination of temperature profile in the central heating domain may simultaneously involve external heating, chemical heat release and conductive heat loss to the ambient. Therefore, an analytical expression for temperature gradient appears to be impossible.

Due to abrupt withdrawal of external heating source, the heat flux by thermal conduction significantly lowers the temperature at the edge of the heating domain, denoted by θ_{edge}. In the absence of chemical reaction, the temperature drop from the center to the edge of heat domain is substantial, i.e., $\left(\theta_{center} - \theta_{edge}\right)/\theta_{center} \sim O(1)$, as shown in figure 3. Accordingly, we may assume that the chemical reaction at $\tilde{r} = 1$ hardly occurs before the arrival of reaction front.

In analogy to equation (40), the profile of temperature in the heating domain can be approximately constituted in the form of an algebraic function, which should satisfy that it has zero gradient at the center due to symmetry and that it is smooth at the edge of the heating domain. Given those conditions, the simplest expression that describes the profile of θ at $\tilde{t} = \tilde{t}_{front}$ can be written in the following form

$$\theta = \left[\left(\frac{\partial\theta}{\partial\tilde{r}}\right)_{\tilde{r}=1} - 2\left(\theta_{edge} - \theta_{front}\right)\right]\tilde{r}^3 + \left[3\left(\theta_{edge} - \theta_{front}\right) - \left(\frac{\partial\theta}{\partial\tilde{r}}\right)_{\tilde{r}=1}\right]\tilde{r}^2 + \theta_{front} \qquad (57)$$

where $(\partial\theta/\partial\tilde{r})_{\tilde{r}=1}$ can be determined by taking derivative of equation (15) with respect to $\tilde{r}$ and then evaluating at $\tilde{t} = \tilde{t}_{front}$, i.e.,

$$\left(\frac{\partial\theta}{\partial\tilde{r}}\right)_{\tilde{r}=1} = \frac{\tilde{Q}_m}{3}\left\{\sqrt{\frac{\tilde{t}_{front}}{\pi}}\left[2\tilde{t}_{front} - 3 + \left(1 - 2\tilde{t}_{front}\right)\exp\left(-\frac{1}{\tilde{t}_{front}}\right)\right] + \operatorname{erf}\left(\frac{1}{\sqrt{\tilde{t}_{front}}}\right) - 1\right\} \qquad (58)$$

Using the constituted temperature profile, given by equation (57), the temperature gradient can be determined, giving

$$\left(\frac{d\theta}{d\tilde{r}}\right)_{\tilde{t}=\tilde{t}_{front}} = \tilde{r}\left[\left(\frac{\partial\theta}{\partial\tilde{r}}\right)_{\tilde{r}=1}(3\tilde{r} - 2) - 6\left(\theta_{edge} - \theta_{front}\right)(\tilde{r} - 1)\right] \qquad (59)$$

Substituting equations (56) and (59) into equation (54) yields the time lapse for the reaction front propagating from the center to the edge of heating domain:

$$\tilde{t}_{propagation} \approx \frac{\theta_{front} - \theta_{edge}}{\tilde{B}\tilde{q}} e^{(1+\theta_a)/(1+\theta_{front})} \qquad (60)$$

where we have used the fact that the temperature at the reaction front is considerably higher than the ambient temperature, i.e., $\theta_{front} \gg 1$, while it is much less than the activation temperature, i.e., $\theta_{front}/\theta_a \ll 1$.

3.5 Formation of the ignition kernel

The arrival of reaction front to the edge of heating domain can be considered as the formation of ignition kernel. Outside the ignition kernel, the reaction front moves into the fresh reactant. This situation identically resembles the initial condition of ignition kernel adopted in existing theoretical studies [13, 21, 22], which considered the development of the ignition kernel and transition to self-sustained spherical flame.

As shown in figure 1, the formation of ignition kernel consists of three sequential stages, i.e., thermal runaway that initiates chemical reaction at $\tilde{r} = 0$, depletion of reactant that generates a reaction front at $\tilde{r} = 0$, and the propagation of the reaction front from $\tilde{r} = 0$ to $\tilde{r} = 1$. The total time lapse of ignition kernel formation, denoted by $\tilde{t}_{kernel}$, is the summation of delay times for each individual process, i.e.,

$$\tilde{t}_{kernel} = \tilde{t}_{explosion} + \tilde{t}_{consumption} + \tilde{t}_{propagation} \qquad (61)$$

The time for thermal runaway $\tilde{t}_{explosion}$ is evaluated by integrating equation (23) numerically, which rigorously considers the transient variation of central temperature due to external heating. By analyzing the temporal variation of Y_{center} based on the numerical solution of equation (48), the flame front generation time $\tilde{t}_{front}$ is specified as the instant when Y_{center} becomes less than 0.1. The time for flame kernel formation $\tilde{t}_{kernel}$ is calculated from the equation (60), which measures the time lapse for the flame front propagating from the heating center to the edge of heating domain driven by local reactivity gradient.

Figure 11 shows that the variations of $\tilde{t}_{front}$ and $\tilde{t}_{kernel}$ are analogous to that of $\tilde{t}_{explosion}$. At relatively low heating power density, $\tilde{t}_{explosion}$, $\tilde{t}_{front}$ and $\tilde{t}_{kernel}$ all increase rapidly. This is because at lower $\tilde{Q}_m$, the effect of conductive heat loss becomes increasingly stronger, which significantly lowers the local reaction rate. At relative large $\tilde{Q}_m$, the gaps between solid lines in figure 11 become increasingly narrow, which indicates that $\tilde{t}_{consumption}$ and $\tilde{t}_{propagation}$ are very short so that the thermal runaway process plays a decisive role in the formation of ignition kernel. It can be understood that the increase in $\tilde{Q}_m$ produces high temperature in the center, which facilitates the chemical reaction there and thereby reduces $\tilde{t}_{consumption}$. Similar arguments apply to $\tilde{t}_{propagation}$. Nevertheless, the decay of $\tilde{t}_{explosion}$ at the rate of $1/\tilde{Q}_m$ needs revision at sufficiently high heating power density, which leads to shock formation and thermal expansion in actual ignition process. Both effects may reduce the chemical reaction rate due to temperature fall and thus make $\tilde{t}_{explosion}$, $\tilde{t}_{front}$ and $\tilde{t}_{kernel}$ become longer.

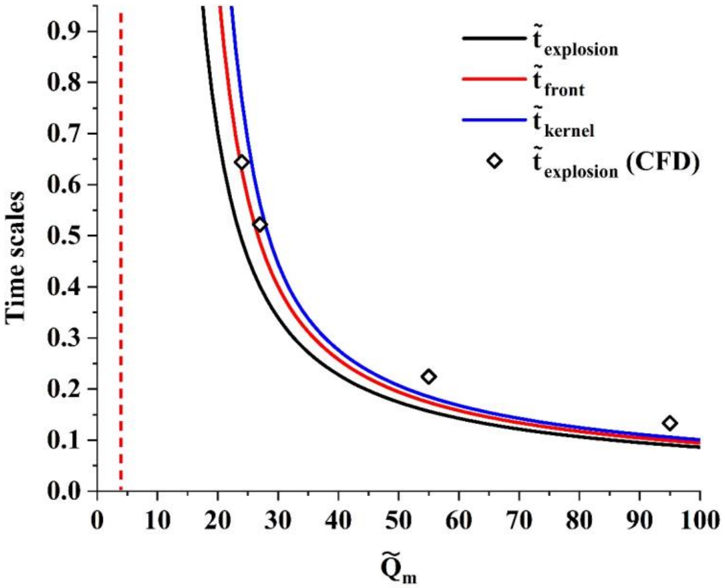

Figure 11 Change of different characteristic time scales with heating power density. The solids lines represent results predicted by theory and the symbols correspond to results from simulation.

To validate the theoretical results, we conduct detailed simulation using the in-house code A-SURF [13, 40] to examine the transient ignition process in a stoichiometric CH_4/air mixture. The mixture is ignited by uniform heating within finite duration of $t_0 = 0.2$ ms and finite spherical domain in the radius of $R_0 = 0.2$ mm. The computational domain is $0 \leq r \leq 50$ cm. Zero gradients of temperature and mass fractions are enforced at both boundaries, r = 0 and 50 cm. The homogeneous mixture is initially static with a temperature of $T = 300$ K and uniformly distributed over the computational domain. The pressure is 1 atm. A-SURF solves the conservation equations (including species, momentum and energy conservation equations) for one-dimensional, adiabatic, multi-component, reactive flow with the finite volume method. The CHEMKIN and TRANSPORT packages [41] are incorporated into A-SURF to calculate the reaction rates as well as thermodynamic and mixture-averaged transport properties. The detailed chemistry, GRI-Mech 3.0 [42] is used in simulation. A-SURF has been successfully used in previous studies on ignition and flame propagation. The details on governing equations and numerical schemes can be found in Chen et al. [13, 40] and thereby are not repeated here.

In simulation, the delay time for thermal runaway $\tilde{t}_{explosion}$ is defined as the instant when the heat release rate due to chemical reaction becomes positive at the center of heating domain. The consumption time of reactant $\tilde{t}_{consumption}$ is measured when the reaction rate reaches the highest value at the center of heating domain, which implies the appearance of reaction front there. The propagation time of the reaction front $\tilde{t}_{propagation}$ is determined as the instant when the highest reaction rate occurs at $r = R_0 = 0.2$ mm.

Four situations with increasing thermal energy deposition, denoted by $E_{heating}$, i.e., $E_{heating}$ =0.15, 0.175, 0.35 and 0.6 mJ are investigated and different time scales depicted in figure 1 are extrapolated. Converting relevant quantities into non-dimensional form according to equation (7), $\tilde{t}_{explosion}$ extrapolated from numerical simulation is plotted in figure 10. It is seen that $\tilde{t}_{explosion}$ from simulation agrees well with theoretical prediction. The quantitative discrepancy may be attributed to that the simplified one-step global reaction model may not be as accurate as the detailed chemical reaction mechanism adopted in simulation. Besides, variation of reference temperature may change the magnitudes of various thermal and transport properties, which also contributes to the difference between theoretical prediction and numerical simulation.

Figure 12 shows that the ratios $\tilde{t}_{front}/\tilde{t}_{explosion}$ and $\tilde{t}_{kernel}/\tilde{t}_{explosion}$ both decrease with $\tilde{Q}_m$. In wide range of heating power density, the theoretically predicted $\tilde{t}_{front}/\tilde{t}_{explosion}$ agrees well with that from simulation. At relatively high $\tilde{Q}_m$, the theoretical prediction slightly underestimates the time scale for ignition kernel formation. Because of complexity during the reaction front propagation, there are different mechanisms leading to such discrepancy. In addition to the simplified one-step global reaction model, the estimation of $\tilde{u}_{front}$ based on the reactivity gradient theory may introduce uncertainty in subsequent calculation of $\tilde{t}_{propagation}$, which shall be discussed as follows. The term $\partial\tilde{t}_{front}/\partial\theta$ interprets the sensitivity of reaction rate with temperature change and it is actually a function of radial coordinate. However, the symmetric condition at the center facilitates thermal energy accumulation there, which makes the reaction front develop more readily. Taking $\partial\tilde{t}_{front}/\partial\theta$ out of the integration in equation (53) hypothesizes that the reaction front formation at every radial distance within the heating domain follows the identical procedure as that at the center. Accordingly, such approximation overestimates the local reaction rate and thus leads to smaller value of $\partial\tilde{t}_{front}/\partial\theta$. Therefore, it yields a larger propagation speed of reaction front and thereby shorter propagation time. Note that we also consider a fuel-lean CH_4/air mixture with the equivalence ratio of 0.6, and good agreement between theory and simulation is also achieved.

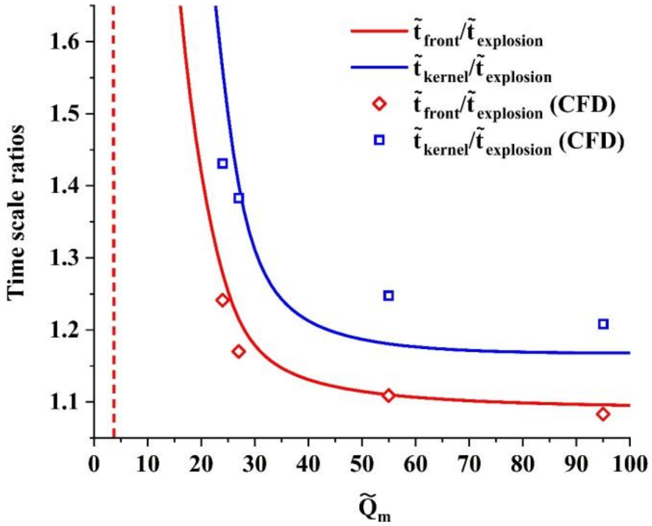

Figure 12 Change of time scale ratios with heating power density. The theoretically predicted $\tilde{t}_{front}/\tilde{t}_{explosion}$ and $\tilde{t}_{kernel}/\tilde{t}_{explosion}$ are represented by red and blue solid lines, respectively. The corresponding ratios obtained via numerical simulation are represented by hollow symbols of diamond and square shapes, respectively.

The time scale analysis suggests that the process of ignition kernel formation is primarily affected by the rate of thermal energy deposition from the external source and the enhanced chemical reaction within the heating domain. The characteristic time scales for individual stages of ignition kernel formation are found to be considerably shorter than the either the conduction or the diffusion time scales. Accordingly, the differential diffusion effect in the reactant mixture measured by the Lewis number tends to show minor impacts before the ignition kernel is fully established. Lewis number is an important parameter in determining the ignition characteristics, such as critical ignition radius and minimum ignition energy. Those parameters are relevant to the evolution of the established ignition kernel (second phase of ignition) rather than the formation of ignition (first phase of ignition). The present work focuses on the ignition kernel formation.

Providing the onset of thermal runaway, the reaction front at the center might be established without external heating, see figure 10. However, it needs longer time to consume the reactant and results in a lower temperature of the reaction front. Figure 13 compares the characteristic times for ignition kernel formation supported by constant heating (solid line) and heating pulse removed at $\tilde{t} = \tilde{t}_{explosion}$ (dash-dot line). According to equation (60), the delay time for the spontaneous propagation of reaction front from $\tilde{r} = 0$ to $\tilde{r} = 1$ would be increased due to reduction of θ_{front}, as indicated by the dash-dotted line in figure 13. The characteristic time for thermal conduction at the edge of heating domain is R_0^2/α, which is equal to unity after non-dimensionalization. Removing external heating at the onset of thermal runaway at the center, the temperature at $\tilde{r} = 1$ falls in the course of time. Denoting the change of θ_{edge} due to thermal conduction by $\Delta\theta_{edge}$, we have $\Delta\theta_{edge}/\theta_{edge} \sim 1 - e^{-\Delta t}$ during a time interval Δt. According to the discussion in defining the FK region, we may hypothesize that a temperature fall of order $O(\epsilon)$, leading to an order $O(1)$ reduction in local reactivity, creates a strong barrier for the passage of the reaction front across the edge of the original heating domain. The time lapse corresponding to such temperature drop can be evaluated by $\Delta t \sim \ln[1/(1-\epsilon)]$. Providing that the reaction front can be established at the center, the propagation time of the reaction front should be shorter than Δt from $\tilde{r} = 0$ to $\tilde{r} = 1$, otherwise, the strong barrier at $\tilde{r} = 1$ may results in flame extinction due to temperature drop. The condition $\tilde{t}_{propagation} < \ln[1/(1-\epsilon)]$ introduces restriction on the ignition kernel formation without support from external heating after onset of thermal runaway. It defines an additional minimum heating power density, denoted by $\tilde{Q}_{cr,kernel}$, below which the heat release from chemical reaction cannot balance with the conductive heat loss, and the reaction front may extinguish during its propagation in the absence of external heating. Regarding the temperature of the propagating reaction front identical to θ_{front}, equation (60) tends to underestimate the propagation time of reaction front. This indicates that the resulting $\tilde{Q}_{cr,kernel}$, indicated by the green dashed line in figure 13, could be a conservative evaluation. The actual threshold heating power density that ensures the spontaneous formation of ignition kernel without external heating after thermal runaway, may still be higher.

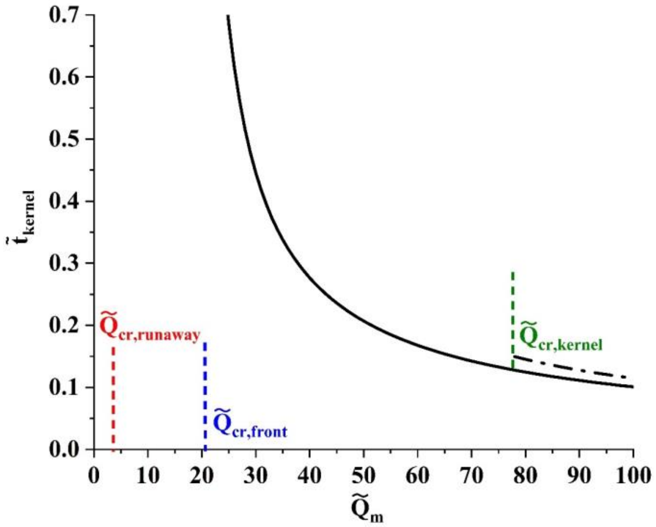

Figure 13 Change of delay time for ignition kernel formation with heating power density. The solid line corresponds to situations in which the thermal energy is constantly delivered during the process of ignition kernel formation, i.e., $\tilde{t}_0 > \tilde{t}_{kernel}$. The dash-dotted line represents the particular situations in which the external heating is removed at the onset of thermal runaway, i.e., $\tilde{t}_0 = \tilde{t}_{explosion}$.

4. Concluding remarks

In this work, theoretical analysis is conducted for the development of ignition kernel in a quiescent flammable mixture subjected to external heating of finite duration in finite domain. Different characteristic time scales (see figure 1) and critical heating powers (see figure 2) involved in the ignition kernel formation are investigated in-detail. Since the analytical treatments are conducted in terms of non-dimensional quantities, the derived results are generally applicable various external heating schemes, represented by duration t_0, domain size R_0, and power density Q_m, and reactants, characterized by activation temperature T_a, combustion heat release q, reaction frequency factor B, thermal diffusivity α and initial temperature T_∞.

Because of drastic change in temperature and mass fraction of reactant, the ignition kernel formation is essentially a transient process, and it consists of three stages: (1) appearance of thermal runaway, (2) onset of reaction front at the center, and (3) propagation of the reaction front to the edge of heating domain. These three stages are associated with characteristic time scales, denoted by $\tilde{t}_{explosion}$, $\tilde{t}_{consumption}$, and $\tilde{t}_{propagation}$, respectively. Figure 1 gives a schematic description to various stages during ignition kernel formation in terms of characteristic time scales. $\tilde{t}_{explosion}$ is evaluated by the Livengood-Wu integral with knowledge of the transient variation of θ_{center}, which can be obtained in analytical expression in the absence of chemical reaction. Subsequent to thermal runaway, chemical reaction is concentrated in the Frank-Kamenetskii region. Integrating the governing equations over the FK region gives a pair of nonlinear ordinary differential equations for θ_{center} and Y_{center}, whose solution helps to determine the characteristic time scale for reactant depletion at the center, $\tilde{t}_{consumption}$. Supported by external heating, the propagating speed of reaction front from $\tilde{r} = 0$ to $\tilde{r} = 1$ is dominated by local reactivity. The characteristic time $\tilde{t}_{propagation}$ is then evaluated by integrating the reactivity gradient over the heating domain according to the gradient theory of Zel'dovich.

The theoretical results are verified by transient simulations considering detailed chemistry and transport. The theoretically predicted time scales agree well with those from simulation. At high heating power densities, the magnitudes of $\tilde{t}_{consumption}$ and $\tilde{t}_{propagation}$ shrinks rapidly because of high reaction rate, and $\tilde{t}_{explosion}$ tends to the primary component in the total time delay for ignition kernel formation, i.e., $\tilde{t}_{kernel} \sim \tilde{t}_{explosion}$. In the situation of $\tilde{Q}_m \to \infty$, the Livengood-Wu integral can be evaluated analytically because of the asymptotic linear dependence of θ_{center} upon $\tilde{t}$. This indicates that $\tilde{t}_{explosion}$ falls with increasing $\tilde{Q}_m$ at a rate slightly slower than $1/\tilde{Q}_m$, which results in nonmonotonic variation of critical ignition energy with heating power density.

In contrast to thermal energy deposition at a point of zero dimension, which leads to the unphysical phenomenon of infinitely high temperature, external heating in finite domain can interpret the fact that thermal runaway never takes place at situations of sufficiently low heating power density. The $\tilde{Q}_{cr,runaway}$ is implicitly determined by setting $\tilde{t}_{explosion} \to \infty$ in the Livengood-Wu integral. Thanks to heat release from chemical reaction by consuming reactant, the reaction front and its propagation could occur in self-sustained manner by removing the external heating after the onset of thermal runaway at the center. For pulses that are switched off at the occurrence of thermal runaway, we can define two additional threshold values of heating power densities, $\tilde{Q}_{cr,front}$ and $\tilde{Q}_{cr,kernel}$, which correspond to the spontaneous creation of reaction front and its passage across $\tilde{r} = 1$, respectively.

It is noted that the present analysis describes the development of ignition kernel in a quiescent environment with simplified one-step global chemistry and using the thermal-diffusive model assuming constant density. These are the limitations of the present model. In future studies, it would be interesting to consider the flow of reactant caused by thermal expansion and simplified thermally sensitive intermediate kinetics (e.g., [24]). Besides, the compressibility of the combustible mixture is not considered in the present study. It would provide further insights on the characteristics of ignition when the effects of shock formation [9] are included in future works.

Acknowledgement

This work was supported by National Natural Science Foundation of China (nos. 52176096 and 52006001).

Declaration of Interests

The authors report no conflict of interest.

References

[1] S. Tsuboi, S. Miyokawa, M. Matsuda, T. Yokomori, N. Iida, Influence of spark discharge characteristics on ignition and combustion process and the lean operation limit in a spark ignition engine, *Appl. Energy* 250 (2019) 617-632.

[2] M. Yao, Z. Zheng, H. Liu, Progress and recent trends in homogeneous charge compression ignition (HCCI) engines, *Prog. Energy Combust. Sci.* 35 (2009) 398-437.

[3] E. Mastorakos, Forced ignition of turbulent spray flames, *Proc Combust Inst.* 36 (2017) 2367-2383.

[4] N. Hayashi, A. Sugiura, Y. Abe, K. Suzuki, Development of ignition technology for dilute combustion engines, *SAE Int. J. Engines* 10 (2017) 984-994.

[5] S. Yu, M. Zheng, Future gasoline engine ignition: A review on advanced concepts, *Int. J. Engine Res.* 22 (2021) 1743-1775.

[6] C. Vázquez-Espí, A. Liñán, Fast, non-diffusive ignition of a gaseous reacting mixture subject to a point energy source, *Combust. Theory Model* 5 (2001) 485-498.

[7] C. Vázquez-Espı, A. Linán, Thermal-diffusive ignition and flame initiation by a local energy source, *Combust. Theory Model* 6 (2002) 297-315.

[8] M. Nguyen, S. Shy, Y. Chen, B. Lin, S. Huang, C. Liu, Conventional spark versus nanosecond repetitively pulsed discharge for a turbulence facilitated ignition phenomenon, *Proc. Combust. Inst.* 38 (2021) 2801-2808.

[9] D. Kassoy, The response of a compressible gas to extremely rapid transient, spatially resolved energy addition: an asymptotic formulation, *J. Eng. Math* 68 (2010) 249-262.

[10] Z. Chen, On the accuracy of laminar flame speeds measured from outwardly propagating spherical flames: Methane/air at normal temperature and pressure, *Combust. Flame* 162 (2015) 2442-2453.

[11] M. Faghih, Z. Chen, The constant-volume propagating spherical flame method for laminar flame speed measurement, *Sci. Bull.* 61 (2016) 1296-1310.

[12] W. Han, P. Dai, X. Gou, Z. Chen, A review of laminar flame speeds of hydrogen and syngas measured from propagating spherical flames, *Applications in Energy and Combustion Science* 1 (2020) 100008.

[13] Z. Chen, M.P. Burke, Y. Ju, On the critical flame radius and minimum ignition energy for spherical flame initiation, *Proc. Combust. Inst.* 33 (2011) 1219-1226.

[14] B. Deshaies, G. Joulin, On the initiation of a spherical flame kernel, *Combust. Sci. Technol.* 37 (1984) 99-116.

[15] Z. Chen, Y. Ju, Theoretical analysis of the evolution from ignition kernel to flame ball and planar flame, *Combust. Theory Model* 11 (2007) 427-453.

[16] Y. Wang, W. Han, Z. Chen, Effects of fuel stratification on ignition kernel development and minimum ignition energy of n-decane/air mixtures, *Proc. Combust. Inst.* 37 (2019) 1623-1630.

[17] X. Chen, W. Peng, P. Gillard, L. Courty, M.L. Sankhe, S. Bernard, Y. Wu, Y. Wang, Z. Chen, Effects of fuel decomposition and stratification on the forced ignition of a static flammable mixture, *Combust. Theory Model* 25 (2021) 813-831.

[18] P. Clavin, Quasi-isobaric ignition near the flammability limits. Flame balls and self-extinguishing flames, *Combust. Flame* 175 (2017) 80-90.

[19] P.D. Ronney, On the mechanisms of flame propagation limits and extinguishment-processes at microgravity, *Symposium (International) on Combustion* 22 (1989) 1615-1623.

[20] Y. Zeldovich, G. Barenblatt, V. Librovich, G. Michviladze, Mathematical theory of combustion and explosion, Moscow, *Science,* (1980).

[21] L. He, Critical conditions for spherical flame initiation in mixtures with high Lewis numbers, *Combust. Theory Model* 4 (2000) 159-172.

[22] D. Yu, Z. Chen, Theoretical analysis on the transient ignition of premixed expanding flame in a quiescent mixture, *J. Fluid Mech.* 924 (2021).

[23] T. Jackson, A. Kapila, D. Stewart, Evolution of a reaction center in an explosive material, *SIAM J Appl Math* 49 (1989) 432-458.

[24] H. Zhang, Z. Chen, Spherical flame initiation and propagation with thermally sensitive intermediate kinetics, *Combust. Flame* 158 (2011) 1520-1531.

[25] A.P. Kelley, G. Jomaas, C.K. Law, Critical radius for sustained propagation of spark-ignited spherical flames, *Combust. Flame* 156 (2009) 1006-1013.

[26] G. Joulin, Point-source initiation of lean spherical flames of light reactants: an asymptotic theory, *Combust Sci Technol* 43 (1985) 99-113.

[27] J. Buckmaster, G. Joulin, Radial propagation of premixed flames and t behavior, *Combust. Flame* 78 (1989) 275-286.

[28] P.D. Ronney, Near-limit flame structures at low Lewis number, *Combust. Flame* 82 (1990) 1-14.

[29] D. Yu, Z. Chen, Theoretical analysis on the forced ignition of a quiescent mixture by repetitive heating pulse, *Proc. Combust. Inst.* 39, (2022) in press, https://doi.org/10.1016/j.proci.2022.06.014.

[30] V. Kurdyumov, A. Sánchez, A. Linan, Heat propagation from a concentrated external energy source in a gas, *J. Fluid Mech.* 491 (2003) 379-410.

[31] W. Zhang, Z. Chen, W. Kong, Effects of diluents on the ignition of premixed H2/air mixtures, *Combust. Flame* 159 (2012) 151-160.

[32] D. Kassoy, The Zeldovich spontaneous reaction wave propagation concept in the fast/modest heating limits, *J. Fluid Mech.* 791 (2016) 439-463.

[33] R. Maly, M. Vogel, Initiation and propagation of flame fronts in lean CH4-air mixtures by the three modes of the ignition spark, *Symposium (international) on combustion* 17 (1979) 821-831.

[34] M. Champion, B. Deshaies, G. Joulin, Relative influences of convective and diffusive transports during spherical flame initiation, *Combust. Flame* 74 (1988) 161-170.

[35] F. Khaled, J. Badra, A. Farooq, Ignition delay time correlation of fuel blends based on Livengood-Wu description, *Fuel* 209 (2017) 776-786.

[36] X. Chen, P. Zhao, P. Dai, Z. Chen, On the prediction of hot spot induced ignition by the Livengood-Wu integral, *Proc. Combust. Inst.* 38 (2021) 4709-4716.

[37] J. Livengood, Correlation of autoignition phenomena in internal combustion engines and rapid compression machines, *Symposium (International) on Combustion* 5 (1955) 347-356.

[38] C.K. Law, Combustion Physics, Cambridge University Press2006.

[39] Y.B. Zeldovich, Regime classification of an exothermic reaction with nonuniform initial conditions, *Combust. Flame* 39 (1980) 211-214.

[40] Z. Chen, M.P. Burke, Y. Ju, Effects of Lewis number and ignition energy on the determination of laminar flame speed using propagating spherical flames, *Proc. Combust. Inst.* 32 (2009) 1253-1260.

[41] R.J. Kee, F.M. Rupley, J.A. Miller, Chemkin-II: A Fortran chemical kinetics package for the analysis of gas-phase chemical kinetics, Sandia National Lab.(SNL-CA), Livermore, CA (United States), 1989.

[42] G.P. Smith, D.M. Golden, M. Frenklach, N.W. Moriarty, B. Eiteneer, M. Goldenberg, C.T. Bowman, R.K. Hanson, S. Song, W. Gardiner Jr, GRI-Mech 3.0, 1999, *URL http://www. me. berkeley. edu/gri_mech*, (2011).